Space Is the Place: Effects of Continuous Spatial Structure on Analysis of Population Genetic Data

C. J. Battey,[1] Peter L. Ralph,[2] and Andrew D. Kern[2]

Institute for Ecology Evolution, Department of Biology, University of Oregon, Eugene, Oregon

ORCID IDs: 0000-0002-9958-4282 (C.J.B.); 0000-0002-9459-6866 (P.L.R.); 0000-0003-4381-4680 (A.D.K.)

ABSTRACT Real geography is continuous, but standard models in population genetics are based on discrete, well-mixed populations. As a result, many methods of analyzing genetic data assume that samples are a random draw from a well-mixed population, but are applied to clustered samples from populations that are structured clinally over space. Here, we use simulations of populations living in continuous geography to study the impacts of dispersal and sampling strategy on population genetic summary statistics, demographic inference, and genome-wide association studies (GWAS). We find that most common summary statistics have distributions that differ substantially from those seen in well-mixed populations, especially when Wright's neighborhood size is < 100 and sampling is spatially clustered. "Stepping-stone" models reproduce some of these effects, but discretizing the landscape introduces artifacts that in some cases are exacerbated at higher resolutions. The combination of low dispersal and clustered sampling causes demographic inference from the site frequency spectrum to infer more turbulent demographic histories, but averaged results across multiple simulations revealed surprisingly little systematic bias. We also show that the combination of spatially autocorrelated environments and limited dispersal causes GWAS to identify spurious signals of genetic association with purely environmentally determined phenotypes, and that this bias is only partially corrected by regressing out principal components of ancestry. Last, we discuss the relevance of our simulation results for inference from genetic variation in real organisms.

KEYWORDS space; population structure; demography; haplotype block sharing; GWAS

THE inescapable reality that biological organisms live, move, and reproduce in continuous geography is usually omitted from population genetic models. However, mates tend to live near to one another and to their offspring, leading to a positive correlation between genetic differentiation and geographic distance. This pattern of "isolation by distance" (Wright 1943) is one of the most widely replicated empirical findings in population genetics (Sharbel *et al.* 2000; Jay *et al.* 2012; Aguillon *et al.* 2017). Despite a long history of analytical work describing the genetics of populations distributed across continuous geography (*e.g.*, Wright 1943; Rousset 1997; Barton *et al.* 2002, 2010; Wilkins and Wakeley 2002; Wilkins 2004; Ringbauer *et al.* 2017; Robledo-Arnuncio and

Rousset 2010), much modern work still describes geographic structure as a set of discrete populations connected by migration (*e.g.*, Wright 1931; Epperson 2003; Rousset and Leblois 2011; Shirk and Cushman 2014; Lundgren and Ralph 2019) or as an average over such discrete models (Petkova *et al.* 2015; Al-Asadi *et al.* 2019). For this reason, most population genetics statistics are interpreted with reference to discrete, well-mixed populations, and most empirical papers analyze variation within clusters of genetic variation inferred by programs like *STRUCTURE* (Pritchard *et al.* 2000) with methods that assume these are randomly mating units.

The assumption that populations are well mixed has important implications for downstream inference of selection and demography. Methods based on the coalescent (Kingman 1982; Wakeley 2009) assume that the sampled individuals are a random draw from a well-mixed population that is much larger than the sample (Wakeley and Takahashi 2003). The key assumption is that the individuals of each generation are *exchangeable*, so that there is no correlation between the fate or fecundity of a parent and that of their offspring (Huillet and Möhle 2013). If dispersal or mate

selection is limited by geographic proximity, this assumption can be violated in many ways. For instance, if mean viability or fecundity is spatially autocorrelated, then limited geographic dispersal will lead to parent–offspring correlations. Furthermore, nearby individuals will be more closely related than an average random pair, so drawing multiple samples from the same area of the landscape will represent a biased sample of the genetic variation present in the whole population (Städler et al. 2009).

Two areas in which spatial structure may be particularly important are demographic inference and genome-wide association studies (GWAS). Previous work has found that discrete population structure can create false signatures of population bottlenecks when attempting to infer demographic histories from microsatellite variation (Chikhi et al. 2010), statistics summarizing the site frequency spectrum (SFS) (Ptak and Przeworski 2002; Städler et al. 2009; St. Onge et al. 2012), or runs of homozygosity in a single individual (Mazet et al. 2015). The increasing availability of whole-genome data has led to the development of many methods that attempt to infer detailed trajectories of population sizes through time based on a variety of summaries of genetic data (Sheehan et al. 2013; Schiffels and Durbin 2014; Liu and Fu 2015; Terhorst et al. 2016). Because all of these methods assume that the populations being modeled are approximately randomly mating, they are likely affected by spatial biases in the genealogy of sampled individuals (Wakeley 1999), which may lead to incorrect inference of population changes over time (Mazet et al. 2015). However, previous investigations of these effects have focused on discrete rather than continuous space models, and the level of isolation by distance at which inference of population size trajectories becomes biased by structure is not well known. Here, we test how two methods suitable for use with large samples of individuals—stairwayplot (Liu and Fu 2015) and SMC++ (Terhorst et al. 2016)—perform when applied to populations evolving in continuous space with varying sampling strategies and levels of dispersal.

Spatial structure is also a major challenge for interpreting the results of GWAS. This is because many phenotypes of interest have strong geographic differences due to the (non-genetic) influence of environmental or socioeconomic factors, which can therefore show spurious correlations with spatially patterned allele frequencies (Mathieson and McVean 2012; Bulik-Sullivan et al. 2015). Indeed, two recent studies found that previous evidence of polygenic selection on human height in Europe was confounded by subtle population structure (Sohail et al. 2018 preprint; Berg et al. 2019), suggesting that existing methods to correct for population structure in GWAS are insufficient. However, we have little quantitative idea of the population and environmental parameters that can be expected to lead to biases in GWAS.

Last, some of the most basic tools of population genetics are summary statistics like F_{IS} and Tajima's D, which are often interpreted as reflecting the influence of selection or demography on sampled populations (Tajima 1989). Statistics like Tajima's D are essentially summaries of the SFS, which itself reflects variation in branch lengths and tree structures of the underlying genealogies of sampled individuals. Geographically limited mate choice distorts the distribution of these genealogies (Maruyama 1972; Wakeley 1999), which can affect the value of Tajima's D (Städler et al. 2009). Similarly, the distribution of tract lengths of identity-by-state among individuals contains information about not only historical demography (Harris and Nielsen 2013; Ralph and Coop 2013) and selection (Garud et al. 2015), but also dispersal and mate choice (Baharian et al. 2016; Ringbauer et al. 2017). We are particularly keen to examine how such summaries will be affected by models that incorporate continuous space, both to evaluate the assumptions underlying existing methods and to identify where the most promising signals of geography lie.

To study this, we have implemented an individual-based model in continuous geography that incorporates overlapping generations, local dispersal of offspring, and density-dependent survival. We simulate chromosome-scale genomic data in tens of thousands of individuals from parameter regimes relevant to common subjects of population genetic investigation, and output the full genealogy and recombination history of all final-generation individuals. We use these simulations to test how sampling strategy interacts with geographic population structure to cause systematic variation in population genetic summary statistics typically analyzed assuming discrete population models. We then examine how the fine-scale spatial structures occurring under limited dispersal impact demographic inference from the SFS. Last, we examine the impacts of continuous geography on GWAS and identify regions of parameter space under which the results from GWAS may be misleading.

Materials and Methods

Modeling evolution in continuous space

The degree to which genetic relationships are geographically correlated depends on the chance that two geographically nearby individuals are close relatives: in modern terms, by the tension between migration (the chance that one is descended from a distant location) and coalescence (the chance that they share a parent). A key early observation by Wright (1946) is that this balance is often nicely summarized by the "neighborhood size," defined in two dimensions to be $N_W = 4\pi\rho\sigma^2$, where σ^2 is one-half of the mean squared parent–offspring distance and ρ is the population density [see Rousset (1997) for further discussion of parameter definitions in one- and two-dimensional habitats]. This can be thought of as proportional to the average number of potential mates for an individual (those within distance 2σ), or the number of potential parents of a randomly chosen individual. Empirical estimates of neighborhood size vary hugely across species; even in human populations, estimates range from 40 to > 5000 depending on the population and method of estimation (Table 1).

Table 1 Neighborhood size estimates from empirical studies

Species	Description	Neighborhood size	Method	Citation
Ipomopsis aggregata	Flowering plant	12.60–37.80	Genetic	Campbell and Dooley (1992)
Borrichia frutescens	Salt marsh plant	20–30	Genetic + survey	Antlfinger (1982)
Oreamnos americanus	Mountain goat	36–100	Genetic	Shirk and Cushman (2014)
Homo sapiens	Gainj- and Kalam-speaking people, Papua New Guinea	40–213	Genetic	Rousset (1997)
Formica sp.	Colonial ants	50–100	Genetic	Pamilo (1983)
Astrocaryum mexicanum	Palm tree	102–895	Genetic + survey	Eguiarte *et al.* (1993)
Spermophilus mollis	Ground squirrel	204–480	Genetic + survey	Antolin *et al.* (2001)
Sceloperus olivaceus	Lizard	225–270	Survey	Kerster (1964)
Dieffenbachia longispatha	Beetle-pollinated colonial herb	227–611	Survey	Young (1988)
A. aegypti	Yellow fever mosquito	268	Genetic	Jasper *et al.* (2019)
Homo sapiens	Gainj- and Kalam-speaking people, Papua New Guinea	410	Survey	Rousset (1997)
Quercus laevis	Oak tree	> 440	Genetic	Berg and Hamrick (1995)
Drosophila pseudoobscura	Fruit fly	500–1000	Survey + crosses	Wright (1946)
Homo sapiens	Population Reference Sample data Northeast Europe	1342–5425	Genetic	Ringbauer *et al.* (2017)

The first approach to modeling continuously distributed populations was to endow individuals in a Wright–Fisher model with locations in continuous space. However, since the total size of the population is constrained, this introduces interactions between arbitrarily distant individuals, which (aside from being implausible) was shown by Felsenstein (1975) to eventually lead to unrealistic population clumping if the range is sufficiently large. Another method for modeling spatial populations is to assume the existence of a grid of discrete randomly mating populations connected by migration, thus enforcing regular population density by edict. Among many other results drawn from this class of "lattice" or stepping-stone model (Epperson 2003), Rousset (1997) showed that the slope of the linear regression of genetic differentiation (F_{ST}) against the logarithm of spatial distance is an estimate of neighborhood size. Although these grid models may be good approximations of continuous geography in many situations, they do not model demographic fluctuations and limit investigation of spatial structure below the level of the deme, assumptions whose impacts are unknown. An alternative method for dealing with continuous geography is a new class of coalescent model, the spatial Λ-Fleming–Viot models (Barton *et al.* 2010; Kelleher *et al.* 2014).

To avoid hard-to-evaluate approximations, we here used forward-time, individual-based simulations across continuous geographical space. The question of what regulates real populations has a long history and many answers (*e.g.*, Lloyd 1967; Antonovics and Levin 1980; Crawley 1990), but it is clear that populations must at some point have density-dependent feedback on population size, or else they would face eventual extinction or explosion. In the absence of unrealistic global population regulation, this regulation must be local, and there are many ways to achieve this (Bolker *et al.* 2003). In our simulations, each individual's probability of survival is a decreasing function of local population density, which shifts reproductive output toward low-density regions, and produces total census sizes that fluctuate around an equilibrium. This also prevents the population clumping seen by Felsenstein (1975) (Supplemental Material, Figure S1). Such models have been used extensively in ecological modeling (Durrett and Levin 1994; Bolker and Pacala 1997; Law *et al.* 2003; Fournier and Méléard 2004; Champer *et al.* 2019 *preprint*), but rarely in population genetics where, to our knowledge, implementations of continuous space models before their availability through SLiM (Haller and Messer 2019) have focused on a small number of genetic loci (*e.g.*, Slatkin and Barton 1989; Barton *et al.* 2002; Robledo-Arnuncio and Rousset 2010; Jackson and Fahrig 2014; Rossine 2014), which limits the ability to investigate the impacts of continuous space on genome-wide genetic variation as is now routinely sampled from real organisms. By simulating chromosome-scale sequence alignments and complete population histories, we are able to treat our simulations as real populations and replicate the sampling designs and analyses commonly conducted on real genomic data.

A forward-time model of evolution in continuous space

We simulated populations using the program SLiM v3.1 (Haller and Messer 2019). Each time step consists of three stages: reproduction, dispersal, and mortality. To reduce the number of parameters we use the same parameter, denoted σ, to modulate the spatial scale of interactions at all three stages by adjusting the SD of the corresponding Gaussian functions. Informally, we think of σ as the "dispersal distance," although only one of those stages is dispersal.

At the beginning of the simulation, individuals are distributed uniformly at random on a continuous, square landscape. Individuals are hermaphroditic, and each time step each

produces a Poisson number of offspring with mean $1/L$. Offspring disperse a Gaussian-distributed distance away from the parent with mean zero and SD σ in both the x and y coordinates. Each offspring is produced with a mate selected randomly from those within distance 3σ, with probability of choosing a neighbor at distance d proportional to the Gaussian density with mean zero and SD σ, which is $g(d) = \exp(-d^2/2\sigma^2)/(2\sigma^2)$.

To maintain a stable population, mortality increases with local population density. To do this, we say that individuals at distance d have a competitive interaction with strength $g(d)$. Then, the sum of all competitive interactions with individual i is $n_i = \sum_j g(d_{ij})$, where d_{ij} is the distance between individuals i and j, and the sum is over all neighbors within distance 3σ. Since g is a probability density, n_i is an estimate of the number of nearby individuals per unit area. Then, given a per-unit carrying capacity K, the probability of survival until the next time step for individual i is

$$p_i = \min\left(0.95, \frac{1}{1 + n_i/(K(1+L))}\right). \quad (1)$$

We choose this functional form so that the equilibrium population density per unit area is close to K, and the mean lifetime is around L; for more description see the Appendix.

An important step in creating any "spatial model" is dealing with range edges. Because local population density is used to model competition, edge or corner populations can be assigned artificially high fitness values because they lack neighbors within their interaction radius but outside the bounds of the simulation. We approximate a decline in habitat suitability near edges by decreasing the probability of survival proportional to the square root of distance to edges in units of σ. The final probability of survival for individual i is then:

$$s_i = p_i \min\left(1, \sqrt{x_i/\sigma}\right)\min\left(1, \sqrt{y_i/\sigma}\right)$$
$$\times \min\left(1, \sqrt{(W-x_i)/\sigma}\right)\min\left(1, \sqrt{(W-y_i)/\sigma}\right) \quad (2)$$

where x_i and y_i are the spatial coordinates of individual i, and W is the width (and height) of the square habitat. This buffer roughly counteracts the increase in fitness that individuals close to the edge would otherwise have, though the effect is relatively subtle (Figure S2).

To isolate spatial effects from other components of the model such as overlapping generations, increased variance in reproductive success, and density-dependent fitness, we also implemented simulations identical to those above, except that mates are selected uniformly at random from the population and offspring disperse to a uniform random location on the landscape. We refer to this model as the "random mating" model, in contrast to the first, spatial model.

We stored the full genealogy and recombination history of final-generation individuals as tree sequences (Kelleher *et al.* 2018), as implemented in SLiM (Haller *et al.* 2019). Scripts for figures and analyses are available at https://github.com/kern-lab/spaceness.

We ran 400 simulations for the spatial and random mating models on a square landscape of width $W = 50$ with per-unit carrying capacity $K = 5$ (census $N \approx 10{,}000$), average lifetime $L = 4$, genome size 10^8 bp, recombination rate 10^{-9} per bp per generation, and drawing σ values from a uniform distribution between 0.2 and 4. To speed up the simulations and limit memory overhead, we used a mutation rate of 0 in SLiM and later applied mutations to the tree sequence with msprime's mutate function (Kelleher *et al.* 2016). Because msprime applies mutations proportionally to elapsed time, we divided the mutation rate of 10^{-8} mutations per site per generation by the average generation time estimated for each value of σ (see "*Demographic parameters*" below) to convert the rate to units of mutations per site per unit time. We verify that this procedure produces the same SFS as applying mutations directly in SLiM in Figure S3, in agreement with theory (Ralph *et al.* 2019b *preprint*). Simulations were run for 1.6 million time steps ($\sim30N$ generations).

We also compared our model's output to a commonly used approximation of continuous space, the stepping-stone model, which we simulated with msprime (Kelleher *et al.* 2016). These results are discussed in detail in the Appendix, but in general we find that the demographic structure of a stepping-stone model can depend strongly on the chosen discretization, and some artifacts of discretization seem to become stronger in the limit of a fine grid. For many summary statistics, finer discretizations (we used a 50×50 grid) produced similar results to the continuous model, but this was not true for others (*e.g.*, F_{IS} and Tajima's D), which differed from the continuous model *more* at finer discretizations.

Demographic parameters

Our demographic model includes parameters that control population density (K), mean life span (L), and dispersal distance (σ). However, nonlinearity of local demographic stochasticity causes actual realized averages of these demographic quantities to deviate from the specified values in a way that depends on the neighborhood size. Therefore, to properly compare to theoretical expectations, we empirically calculated these demographic quantities in simulations. We recorded the census population size in all simulations, and used mean population density (ρ, census size divided by total area) to compute neighborhood size as $N_W = 4\pi\rho\sigma^2$. To estimate generation times, we stored ages of the parents of every new individual born across 200 time steps, after a 100 generation burn-in, and took the mean. To estimate variance in offspring number, we tracked the lifetime total number of offspring for all individuals for 100 time steps following a 100-time step burn-in period, and calculated the variance in number of offspring across all individuals in time steps 50–100. All calculations were performed with information recorded in the tree sequence, using pyslim (Ralph *et al.* 2019a).

Note that σ controls the dispersal of offspring away from only *one* parent (*e.g.*, the seed parent for plants), while population genetics usually defines dispersal distance to be the distance to one of the two parents randomly chosen (thus taking into account the distance from pollen parent as well). This second component, the distance between mates, has in our simulations a distribution that is of order σ but that depends on the population's patchiness. If both the between-mate and dispersal distance have variance σ^2 along each axis, then the mean squared distance to a randomly chosen parent along that axis would be $(\sigma^2 + 2\sigma^2)/2 = 3\sigma^2/2$. To match theory, neighborhood size should be defined in terms of *effective* dispersal distance, *i.e.*, the mean squared displacement along an axis between parent–child pairs found moving back along a lineage (Barton *et al.* 2002), and *effective* population density (Rousset 1997). However, we use σ and ρ as defined here to compute N_W because these quantities are more easily observable in practice than their effective versions.

Sampling

Our model records the genealogy and sequence variation of the complete population, but in real data, genotypes are only observed from a relatively small number of sampled individuals. We modeled three sampling strategies similar to common data collection methods in empirical genetic studies (Figure 1). Random sampling selects individuals at random from across the full landscape, "point sampling" selects individuals proportional to their distance from four equally spaced points on the landscape, and midpoint sampling selects individuals in proportion to their distance from the middle of the landscape. Downstream analyses were repeated across all sampling strategies.

Summary statistics

We calculated the SFS and a set of 18 summary statistics (Table S1) from 60 diploid individuals sampled from the final generation of each simulation using the python package scikit-allel (Miles and Harding 2017). Statistics included common single-population summaries including mean pairwise divergence (π), inbreeding coefficient (F_{IS}), and Tajima's *D*, as well as [motivated by the results of Rousset (1997)] the correlation coefficient between the logarithm of the spatial distance and the proportion of identical base pairs across pairs of individuals.

Following recent studies that showed strong signals for dispersal and demography in the distribution of shared haplotype block lengths (*e.g.*, Baharian *et al.* 2016; Ringbauer *et al.* 2017), we also calculated various summaries of the distribution of pairwise identical-by-state (IBS) block lengths among sampled chromosomes, defined to be the set of distances between adjacent sites that differ between the two chromosomes. The full distribution of lengths of IBS tracts for each pair of chromosomes was first calculated with a custom python function. We then calculated the first three moments of this distribution (mean, variance, and skew) and the
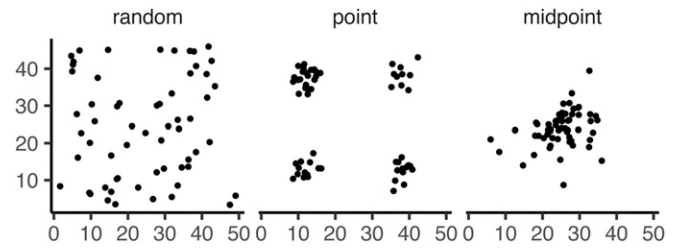

Figure 1 Example sampling maps for 60 individuals on a 50×50 landscape for midpoint, point, and random sampling strategies, respectively.

number of blocks over 10^6 bp both for each pair of individuals and for the full distribution across all pairwise comparisons. We then calculated correlation coefficients between spatial distance and each moment of the pairwise IBS tract distribution. Because more closely related individuals on average share longer haplotype blocks, we expect that spatial distance will be negatively correlated with mean haplotype block length and that this correlation will be strongest (*i.e.*, most negative) when dispersal is low. The variance, skew, and counts of long haplotype block statistics are meant to reflect the relative length of the right (upper) tail of the distribution, which represents the frequency of long haplotype blocks and so should reflect recent demographic events (Chapman and Thompson 2002). For a subset of simulations, we also calculated cumulative distributions for IBS tract lengths across pairs of distant (> 40 map units) and nearby (< 10 map units) individuals. Last, we examined the relationship between allele frequency and the spatial dispersion of an allele by calculating the average distance between individuals carrying each derived allele.

The effects of sampling on summary statistic estimates were summarized by testing for differences in mean [ANOVA; R Core Team (2018)] and variance [Levene's test; Fox and Weisberg (2011)] across sampling strategies for each summary statistic.

Demographic inference

To assess the impacts of continuous spatial structure on demographic inference, we inferred population size histories for all simulations using two approaches: stairwayplot (Liu and Fu 2015) and SMC++ (Terhorst *et al.* 2016). Stairwayplot fits its model to a genome-wide estimate of the SFS, while SMC++ also incorporates linkage information. For both methods, we sampled 20 individuals from all spatial simulations using random, midpoint, and point sampling strategies.

As recommended by its documentation, we used stairwayplot to fit models with multiple bootstrap replicates drawn from empirical genomic data, and took the median inferred N_e per unit time as the best estimate. We calculated each SFS with scikit-allel (Miles and Harding 2017), generated 100 bootstrap replicates per simulation by resampling over sites, and fitted models for all bootstrap samples using default settings.

For SMC++, we first output genotypes as VCF with msprime and then used SMC++'s standard pipeline for preparing input files assuming no polarization error in the SFS. We used the first individual in the VCF as the "designated individual" when fitting models, and allowed the program to estimate the recombination rate during optimization. We fitted models using the "estimate" command rather than the now-recommended cross-validation approach because our simulations had only a single contig.

To evaluate the performance of these methods, we binned simulations by neighborhood size, and took a rolling median of inferred N_e trajectories across all model fits in a bin for each method and sampling strategy. We also examined how varying levels of isolation by distance impacted the variance of N_e estimates by calculating the SD of N_e from each best-fit model.

Association studies

To assess the degree to which spatial structure confounds GWAS, we simulated four types of nongenetic phenotype variation for 1000 randomly sampled individuals in each spatial SLiM simulation and conducted a linear regression GWAS with principal components (PCs) as covariates in PLINK (Purcell *et al.* 2007). SNPs with a minor allele frequency (MAF) < 0.5% were excluded from this analysis. Phenotype values were set to vary by 2 SD across the landscape in a rough approximation of the variation seen in height across Europe (Garcia and Quintana-Domeque 2006, 2007; Turchin *et al.* 2012). Conceptually, our approach is similar to that taken by Mathieson and McVean (2012), though here we model fully continuous spatial variation and compare GWAS outputs across a range of dispersal distances.

In all simulations, the phenotype of each individual is determined by drawing from a Gaussian distribution with SD 10 and a mean that may depend on spatial position. In spatially varying models, the mean phenotype differs by 2 SD across the landscape. We then adjust the geographic pattern of mean phenotype to create four types of spatially autocorrelated environmental influences on phenotype. In the first simulation of *nonspatial* environments, the mean did not change, so that all individuals' phenotypes were drawn independently from a Gaussian distribution with mean 110 and SD 10. Next, to simulate *clinal* environmental influences on phenotype, we increased the mean phenotype from 100 on the left edge of the range to 120 on the right edge (two phenotypic SDs). Concretely, the mean phenotype p for an individual at position (x, y) is $p = 100 + 2x/5$. Third, we simulated a more concentrated "corner" environmental effect by setting the mean phenotype to 120 for individuals with both x and y coordinates below 20 (2 SD above the rest of the map). Finally, in "patchy" simulations we selected 10 random points on the map and set the mean phenotype of all individuals within three map units of each of these points to 120.

We performed PC analysis (PCA) using scikit-allel (Miles and Harding 2017) on the matrix of derived allele counts by individual for each simulation. SNPs were first filtered to remove strongly linked sites by calculating linkage disequilibrium (LD) between all pairs of SNPs in a 200-SNP moving window and dropping one of each pair of sites with an $R^2 > 0.1$. The LD-pruned allele count matrix was then centered and all sites scaled to unit variance when conducting the PCA, following recommendations in Patterson *et al.* (2006).

We ran linear-model GWAS both with and without the first 10 PCs as covariates in PLINK, and summarized results across simulations by counting the number of SNPs with P-values < 0.05 after adjusting for an expected false-positive rate of < 5% (Benjamini and Yekutieli 2001). We also examined P-values for systematic inflation by comparing them with the values expected from a uniform distribution (because no SNPs were used when generating phenotypes, well-calibrated P-values should be uniform).

Results from all analyses were summarized and plotted with the "ggplot2" (Wickham 2016) and "cowplot" (Wilke 2019) packages in R (R Core Team 2018).

Data availability

Scripts used for all analyses and figures are available at ⑩ https://github.com/kern-lab/spaceness. Supplemental material available at figshare: https://doi.org/10.25386/genetics.12019008.

Results

Demographic parameters and run times

Adjusting the spatial dispersal and interaction distance, σ, has a surprisingly large effect on demographic quantities that are usually fixed in Wright–Fisher models: the generation time, census population size, and variance in offspring number, as shown in Figure 2. Because our simulation is parameterized on an individual level, these population parameters emerge as a property of the interactions among individuals rather than being directly set. Variation across runs occurs because, even though the parameters K and L that control population density and mean lifetime, respectively, were the same in all simulations, the strength of stochastic effects depends strongly on the spatial interaction distance σ. For instance, the population density near to individual i (denoted n_i above) is computed by averaging over roughly $N_W = 4\pi K\sigma^2$ individuals, and so has SD proportional to $1/\sqrt{N_W}$; it is more variable at lower densities (recall that N_W is Wright's neighborhood size). Since the probability of survival is a nonlinear function of n_i, actual equilibrium densities and lifetimes differ from K and L. This is the reason that we included random mating simulations, where mate choice and offspring dispersal are both nonspatial, since this should preserve the random fluctuations in local population density while destroying any spatial genetic structure. We verified that random mating models retained no geographic signal by showing that summary statistics did not differ significantly between sampling regimes (Table S2), unlike in spatial models (discussed below).
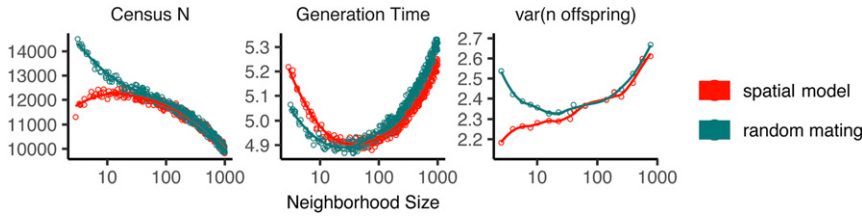
Figure 2 Genealogical parameters from spatial and random mating SLiM simulations, by neighborhood size.

There are a few additional things to note about Figure 2. First, all three quantities are nonmonotone with neighborhood size. Census size largely declines as neighborhood size increases for both the spatial and random mating models. However, for spatial models this decline only begins for neighborhood size ≥10. Spatial and random mating models are indistinguishable from one another for neighborhood sizes > 100. Census sizes range from ∼14,000 at low σ in the random mating model to 10,000 for both models when neighborhood sizes approach 1000. The scaling of census sizes in both random mating and spatial models appears to be related to two consequences of the spatial competition function: the decline of fitness at range edges, which effectively reduces the habitable area by one σ around the edge of the map and so results in a smaller habitable area at high σ values; and variation in the equilibrium population density given varying competition radii. Furthermore, census size increases in spatial models as neighborhood size increases from 2 to 10. This may reflect an Allee effect (Allee *et al.* 1949), in which some individuals are unable to find mates when the mate selection radius is very small.

Generation time similarly shows complex behavior with respect to neighborhood sizes, and varies between 5.2 and 4.9 time steps per generation across the parameter range explored. Under both the spatial and random mating models, generation time reaches a minimum at a neighborhood size of ∼50. Interestingly, under the range of neighborhood sizes that we examined, generation times between the random mating and spatial models are never quite equivalent; presumably this would cease to be the case at neighborhood sizes higher than we simulated here.

Last, we looked at the variance in number of offspring, a key parameter determining the effective population size. Surprisingly, the spatial and random mating models behave quite differently: while the variance in offspring number increases nearly monotonically under the spatial model, the random mating model actually shows a decline in the variance in offspring number until a neighborhood size of ∼10, before it increases and eventually equals what we observe in the spatial case.

Run times for our model scale approximately linearly with neighborhood size (Figure 3), with the lowest neighborhood sizes reaching 30N generations in around a day and those with neighborhood size approaching 1000 requiring up to 3 weeks of computation. As currently implemented, running simulations at neighborhood sizes > 1000 to coalescence is likely impractical, though running these models for more limited timescales and then "recapitating" the simulation using reverse-time simulation from the resulting tree sequence in msprime is possible (Haller *et al.* 2019).

Impacts of continuous space on population genetic summary statistics

Even though certain aspects of population demography depend on the scale of spatial interactions, it still could be that population genetic variation is well described by a well-mixed population model. Indeed, mathematical results suggest that genetic variation in some spatial models should be well approximated by a Wright–Fisher population if neighborhood size is large and all samples are geographically widely separated (Wilkins 2004; Zähle *et al.* 2005). However, the behaviors of most common population genetic summary statistics other than Tajima's D (Städler *et al.* 2009) have not yet been described in realistic geographic models. Moreover, as we will show, spatial sampling strategies can affect summaries of genetic variation at least as strongly as the underlying population dynamics.

SFS and summaries of diversity

Figure 4 shows the effect of varying neighborhood size and sampling strategy on the SFS (Figure 4 and Figure S5) and several standard population genetic summary statistics (Figure 4B; additional statistics are shown in Figure S4). Consistent with findings in island and stepping-stone simulations (Städler *et al.* 2009), the SFS shows a significant enrichment of intermediate frequency variants in comparison to the nonspatial expectation. This bias is most pronounced below a neighborhood size of 100, and is exacerbated by midpoint and point sampling of individuals (depicted in Figure 1). Reflecting this, Tajima's D is quite positive in the same situations (Figure 4B). Notably, the point at which Tajima's D approaches 0 differs strongly across sampling strategies, varying from a neighborhood size of roughly 50 for random sampling to ≥ 1000 for midpoint sampling.

One of the most commonly used summaries of variation is Tajima's summary of nucleotide diversity, θ_π, calculated as the mean density of nucleotide differences averaged across pairs of samples. As can be seen in Figure 4B, θ_π in the spatial model is inflated by up to threefold relative to the random mating model. This pattern is opposite to the expectation from census population size (Figure 2), because the spatial model has *lower* census size than the random mating model at neighborhood sizes < 100. Differences between these models likely occur because θ_π is a measure of mean time
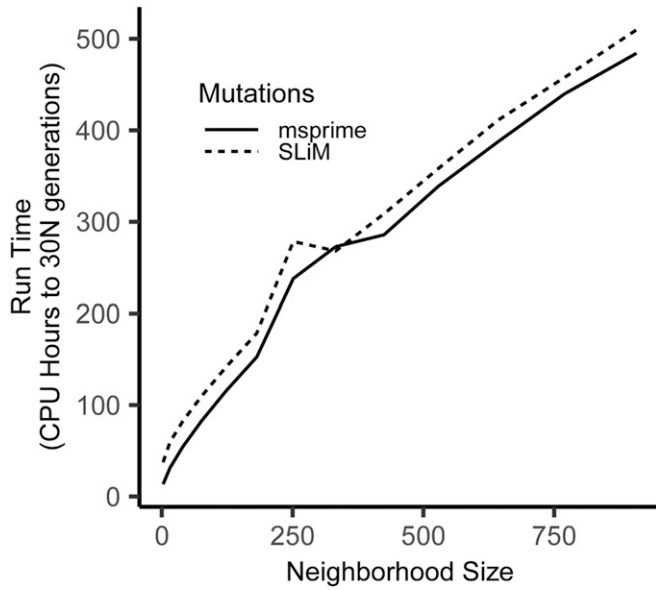
Figure 3 Run times of continuous space simulations with landscape width 50 and expected density 5 under varying neighborhood size. Times are shown for simulations run with mutations applied directly in SLiM (dashed lines) or later applied to tree sequences with msprime (solid lines). Times for simulations run with tree sequence recording disabled are shown in gray. CPU, central processor unit.

to most recent common ancestor between two samples, and at small values of σ, the time for dispersal to mix ancestry across the range exceeds the mean coalescent time under random mating (for instance, at the smallest value of $\sigma = 0.2$, the range is 250 dispersal distances wide, and since the location of a diffusively moving lineage after k generations has variance $k\sigma^2$, it takes $\sim250^2 = 62,500$ generations to mix across the range, which is roughly 10 times larger than the random mating effective population size). θ_π using each sampling strategy approaches the random mating expectation at its own rate, but by a neighborhood size of ~100 all models are roughly equivalent. Interestingly, the effect of sampling strategy is reversed relative to that observed in Tajima's D; midpoint sampling reaches random mating expectations around neighborhood size 50, while random sampling is inflated until around neighborhood size 100.

Values of observed heterozygosity and its derivative F_{IS} also depend heavily on neighborhood size under spatial models as well as the sampling scheme. F_{IS} is inflated above the expectation across most of the parameter space examined and across all sampling strategies. This effect is caused by a deficit of heterozygous individuals in low-dispersal simulations, a continuous-space version of the Wahlund effect (Wahlund 1928). Indeed, for random sampling under the spatial model, F_{IS} does not approach the random mating equivalent until neighborhood sizes of nearly 1000. On the other hand, the dependency of raw observed heterozygosity on neighborhood size is not monotone. Under midpoint sampling, observed heterozygosity is inflated even over the

random mating expectation, as a result of the higher proportion of heterozygotes occurring in the middle of the landscape (Figure S6). This echoes a report from Shirk and Cushman (2014), who observed a similar excess of heterozygosity in the middle of the landscape when simulating under a lattice model.

IBS tracts and correlations with geographic distance

We next turn our attention to the effect of geographic distance on haplotype block length sharing, summarized for sets of nearby and distant individuals in Figure 5. There are two main patterns to note. First, nearby individuals share more long IBS tracts than distant individuals (as expected because they are on average more closely related). Second, the difference in the number of long IBS tracts between nearby and distant individuals decreases as neighborhood size increases. This reflects the faster spatial mixing of populations with higher dispersal, which breaks down the correlation between the IBS tract length distribution and geographic distance. This can also be seen in the bottom row of Figure 4B, where the correlation coefficients between the summaries of the IBS tract length distribution (the mean, skew, and count of tracts $> 10^6$ bp) and geographic distance approaches 0 as neighborhood size increases.

The patterns observed for correlations of IBS tract lengths with geographic distance are similar to those observed in the more familiar correlation of allele frequency measures such as D_{xy} (i.e., "genetic distance") or F_{ST} against geographic distance (Rousset 1997). D_{xy} is positively correlated with the geographic distance between the individuals, and the strength of this correlation declines as dispersal increases (Figure 4B), as expected (Wright 1943; Rousset 1997). This relationship is very similar across random and point sampling strategies, but is weaker for midpoint sampling, perhaps due to a dearth of long-distance comparisons. In much of empirical population genetics, a regression of genetic differentiation against spatial distance is a *de facto* metric of the significance of isolation by distance. The similar behavior of moments of the pairwise distribution of IBS tract lengths shows why haplotype block sharing has recently emerged as a promising source of information on spatial demography, through methods described in Ringbauer *et al.* (2017) and Baharian *et al.* (2016).

Spatial distribution of allele copies

Mutations occur in individuals and spread geographically over time. Because low-frequency alleles generally represent recent mutations (Sawyer 1977; Griffiths *et al.* 1999), the geographic spread of an allele may covary along with its frequency in the population. To visualize this relationship, we calculated the average distance among individuals carrying a focal derived allele across simulations with varying neighborhood sizes, shown in Figure 6. On average, we find that low-frequency alleles are the most geographically restricted, and that the extent to which geography and allele frequency are related depends on the amount of dispersal in
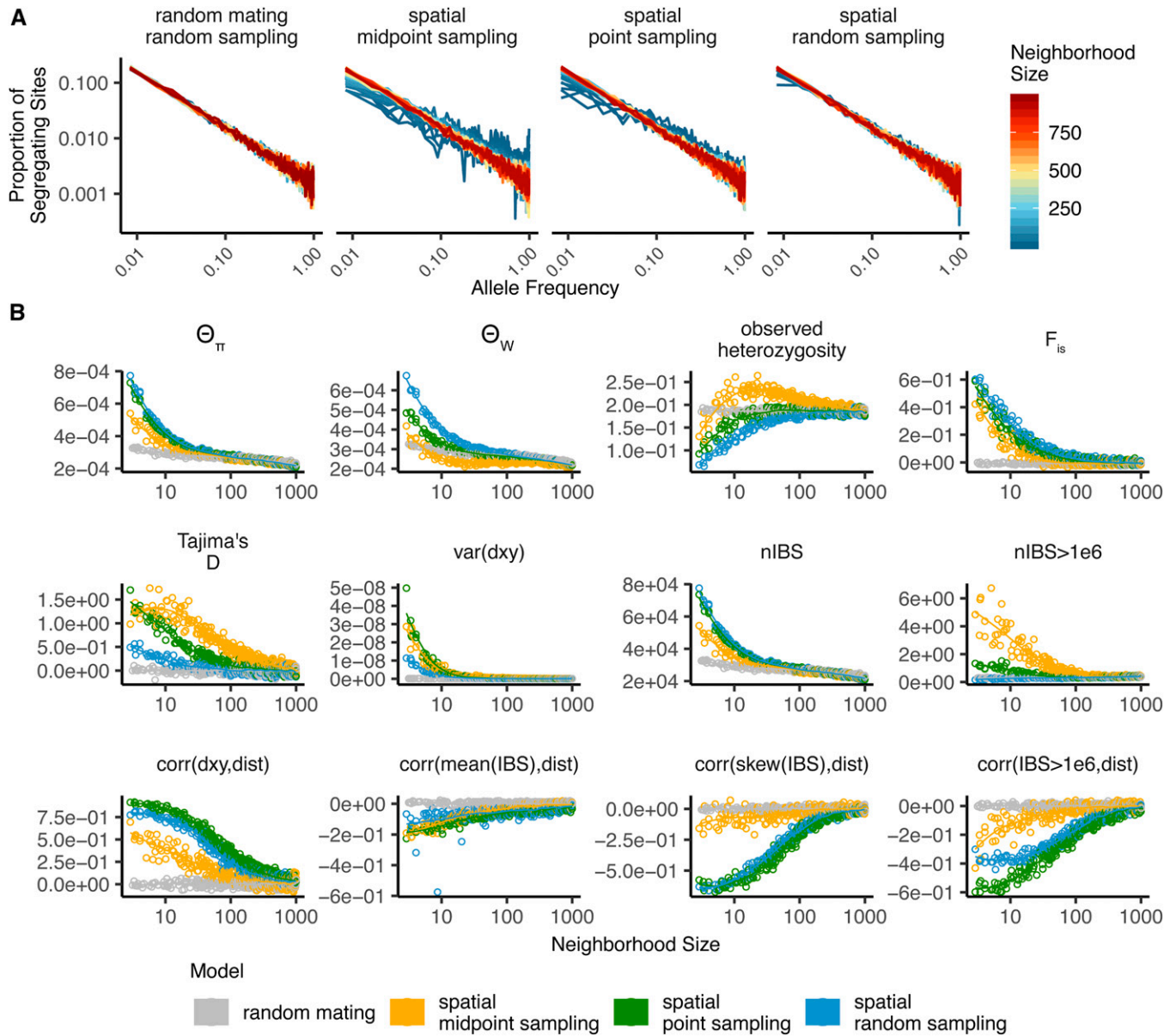
861
862
863
864
865
866
867
868
869
870
871

Figure 4 Site frequency spectrum (A) (note axes are log-scaled) and summary statistic distributions (B) by sampling strategy and neighborhood size. corr, correlation; dist, distance; IBS, identical-by-state; var, variation

the population. For populations with large neighborhood sizes we found that even very low-frequency alleles can be found across the full landscape, whereas in populations with low neighborhood sizes the relationship between distance among allele copies and their frequency is quite strong. This is the basic process underlying Novembre and Slatkin's (2009) method for estimating dispersal distances based on the distribution of low-frequency alleles, and also generates the greater degree of bias in GWAS effect sizes for low-frequency alleles identified in Mathieson and McVean (2012).

Effects of space on demographic inference

One of the most important uses for population genetic data is inferring the demographic history of populations. As demonstrated above, the SFS and the distribution of IBS tracts varies across neighborhood sizes and sampling strategies. Does this variation lead to different inferences of past population sizes? To ask this, we inferred population size histories from samples drawn from our simulated populations with two approaches: stairwayplot (Liu and Fu 2015), which uses a genome-wide estimate of the SFS, and SMC++ (Terhorst *et al.* 2016), which incorporates information on both the SFS and LD across the genome.

Figure 7A shows rolling medians of inferred population size histories from each method across all simulations, grouped by neighborhood size and sampling strategy. In general, these methods tend to slightly overestimate ancient population sizes and infer recent population declines when
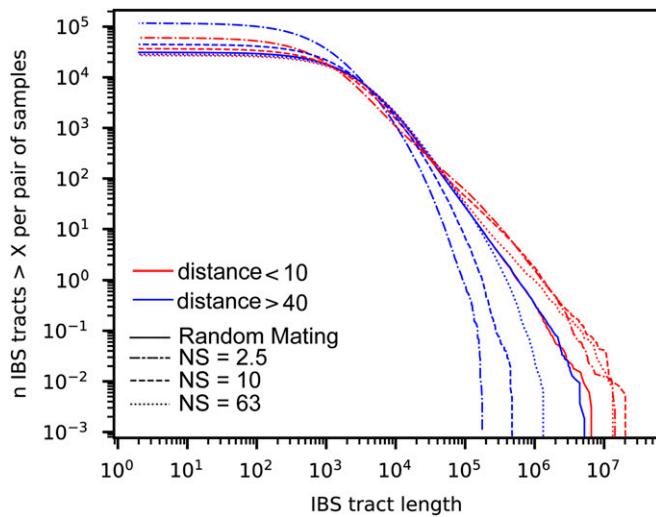
Figure 5 Cumulative distributions for IBS tract lengths per pair of individuals at different geographic distances, across three NSs. Nearby pairs (red curves) share many more long IBS tracts than do distant pairs (blue curves), except in the random mating model. The distributions of long IBS tracts between nearby individuals are very similar across NSs, but distant individuals are much more likely to share long IBS tracts at high NS than at low NS. IBS, identical-by-state; NS, neighborhood size.

neighborhood sizes are < 20 and sampling is spatially clustered. However, the overestimation of ancient population sizes is relatively minor, averaging around a twofold inflation at 10,000 generations before being present in the worst-affected bins. For stairwayplot, we found that many runs infer dramatic population bottlenecks in the last 1000 generations when sampling is spatially concentrated, resulting in 10-fold or greater underestimates of recent population sizes. However SMC++ appeared more robust to this error, with runs on point- and midpoint-sampled simulations at the lowest neighborhood sizes underestimating recent population sizes by roughly one-half, and those on randomly sampled simulations showing little error. Above neighborhood sizes of ~ 100, both methods performed relatively well when averaging across results from multiple simulations.

However, individual simulations were often inferred to have turbulent demographic histories, as shown by the individually inferred histories (shown in Figure S7). Indeed, the SD of inferred N_e across time points (shown in Figure 7B) often exceeds the expected N_e for both methods. That is, despite the nearly constant population sizes in our simulations, both methods tended to infer large fluctuations in population size over time, which could potentially result in incorrect biological interpretations. On average, the variance of inferred population sizes is elevated at the lowest neighborhood sizes and declines as dispersal increases, with the strongest effects seen in stairwayplot results with clustered sampling and neighborhood sizes < 20 (Figure 7B).

GWAS

To ask what confounding effects spatial genetic variation might have on GWAS, we performed GWAS on our simulations using phenotypes that were determined solely by the environment, so any SNP showing statistically significant correlation with a phenotype was a false positive. As expected, spatial autocorrelation in the environment causes spurious associations across much of the genome if no correction for genetic relatedness among samples is performed (Figure 8 and Figure S8). This effect is particularly strong for clinal and corner environments, for which the lowest dispersal levels cause $> 60\%$ of SNPs in the sample to return significant associations. Patchy environmental distributions, which are less strongly spatially correlated (Figure 8A), cause fewer false positives overall but still produce spurious associations at roughly 10% of sites at the lowest neighborhood sizes. Interestingly we also observed a small number of false positives in roughly 3% of analyses on simulations with nonspatial environments, both with and without PC covariates included in the regression.

The confounding effects of geographic structure are well known, and it is common practice to control for this by including PCs as covariates to control for these effects. This mostly works in our simulations: after incorporating the first 10 PC axes as covariates, the vast majority of SNPs no longer surpass a significance threshold chosen to have a 5% false discovery rate (FDR). However, a substantial number of SNPs—up to 1.5% at the lowest dispersal distances—still surpass this threshold (and thus would be false positives in a GWAS), especially under corner and patchy environmental distributions (Figure 8C). At neighborhood sizes > 500, up to 0.31% of SNPs were significant for corner and clinal environments. Given an average of 132,000 SNPs across simulations after MAF filtering, this translates to ≤ 382 false-positive associations; for human-sized genomes, this number would be much larger. In most cases the P-values for these associations were significant after FDR correction but would not pass the threshold for significance under the more conservative Bonferroni correction (see example Manhattan plots in Figure S8).

Clinal environments cause an interesting pattern in false positives after PC correction: at low neighborhood sizes the correction removes nearly all significant associations, but at neighborhood sizes > 250 the proportion of significant SNPs increases to $\leq 0.4\%$ (Figure 8). This may be due to a loss of descriptive power of the PCs; as neighborhood size increases, the total proportion of variance explained by the first 10 PC axes declines from roughly 10–4% (Figure 8B). Essentially, PCA seems unable to effectively summarize the weak population structure present in large-neighborhood simulations given the sample sizes we tested, but these populations continue to have enough spatial structure to create significant correlations between genotypes and the environment. A similar process can also be seen in the corner phenotype distribution, in which the count of significant SNPs initially
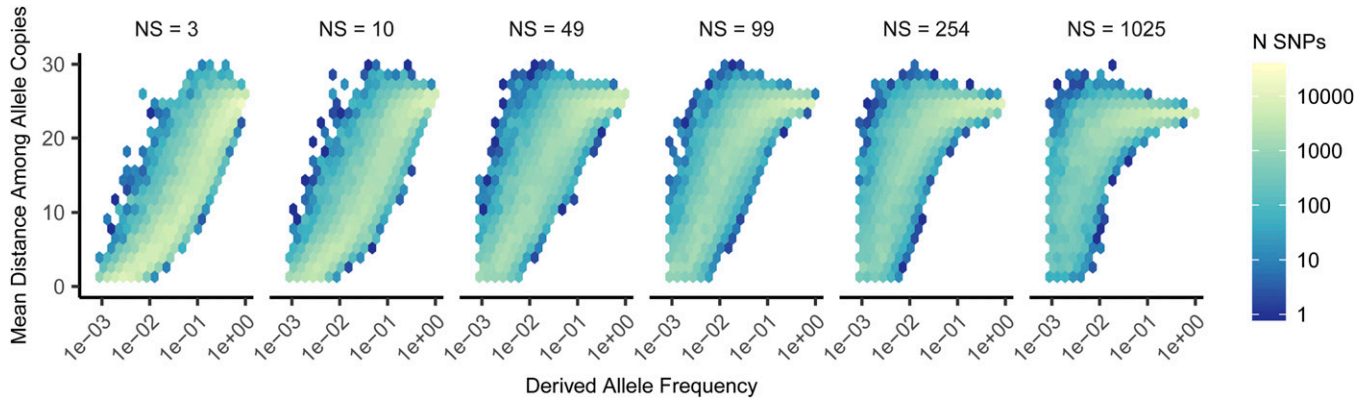
Figure 6 Spatial spread of rare alleles by NS. Each plot shows the distribution (across derived alleles and simulations) of average pairwise distance between individuals carrying a focal derived allele and derived allele frequency. NS, neighborhood size.

declines as neighborhood size increases and then increases at approximately the point at which the proportion of variance explained by PCA approaches its minimum.

Figure 8D shows quantile–quantile plots for a subset of simulations that show the degree of genome-wide inflation of test statistics in PC-corrected GWAS across all simulations and environmental distributions. An alternate visualization is also included in Figure S9. For clinal environments, $-\log_{10}(p)$ values are most inflated when neighborhood sizes are large, consistent with the pattern observed in the count of significant associations after PC regression. In contrast, corner and patchy environments cause the greatest inflation in $-\log_{10}(p)$ at neighborhood sizes < 100, which likely reflects the inability of PCA to account for fine-scale structure caused by very limited dispersal. Finally, we observed that PC regression appears to overfit to some degree for all phenotype distributions, visible in Figure 8D as points falling below the 1:1 line.

Discussion

In this study, we have used efficient forward-time population genetic simulations to describe the myriad influences of continuous geography on genetic variation. In particular, have we examined how three main types of downstream empirical inference are affected by unmodeled spatial population structure: population genetic summary statistics, inference of population size history, and GWAS. As discussed above, space often matters (and sometimes dramatically), both because of how samples are arranged in space and because of the inherent patterns of relatedness established by geography.

Effects of dispersal

Limited dispersal inflates effective population size, creates correlations between genetic and spatial distances, and introduces strong distortions in the SFS that are reflected in a positive Tajima's D (Figure 4). At the lowest dispersal distances, this can increase genetic diversity threefold relative to random mating expectations. These effects are strongest

when neighborhood sizes are < 100, but in combination with the effects of nonrandom sampling they can persist up to neighborhood sizes of $\geq$ 1000 (*e.g.*, inflation in Tajima's D and observed heterozygosity under midpoint sampling). If samples are chosen uniformly from across space, the general pattern is similar to expectations of the original analytic model of Wright (1943), which predicts that populations with neighborhood sizes < 100 will differ substantially from random mating, while those above 10,000 will be nearly indistinguishable from panmixia.

The patterns observed in sequence data reflect the effects of space on the underlying genealogy. Nearby individuals coalesce rapidly under limited dispersal and so are connected by short branch lengths, while distant individuals take much longer to coalesce than they would under random mating. Mutation and recombination events in our simulation both occur at a constant rate along branches of the genealogy, so the genetic distance and number of recombination events separating sampled individuals simply gives a noisy picture of the genealogies connecting them. Tip branches (*i.e.*, branches subtending only one individual) are then relatively short, and branches in the middle of the genealogy connecting local groups of individuals are relatively long, leading to the biases in the SFS shown in Figure 4.

The genealogical patterns introduced by limited dispersal are particularly apparent in the distribution of haplotype block lengths (Figure 4). This is because IBS tract lengths reflect the impacts of two processes acting along the branches of the underlying genealogy, both mutation and recombination, rather than just mutation, as is the case when looking at the SFS or related summaries. This means that the pairwise distribution of haplotype block lengths carries with it important information about genealogical variation in the population, and correlation coefficients between moments of this distribution and geographic location contain signals similar to the correlations between F_{ST} or D_{xy} and geographic distance (Rousset 1997). Indeed, this basic logic underlies two recent studies explicitly estimating dispersal from the distribution of shared haplotype block lengths (Baharian *et al.*
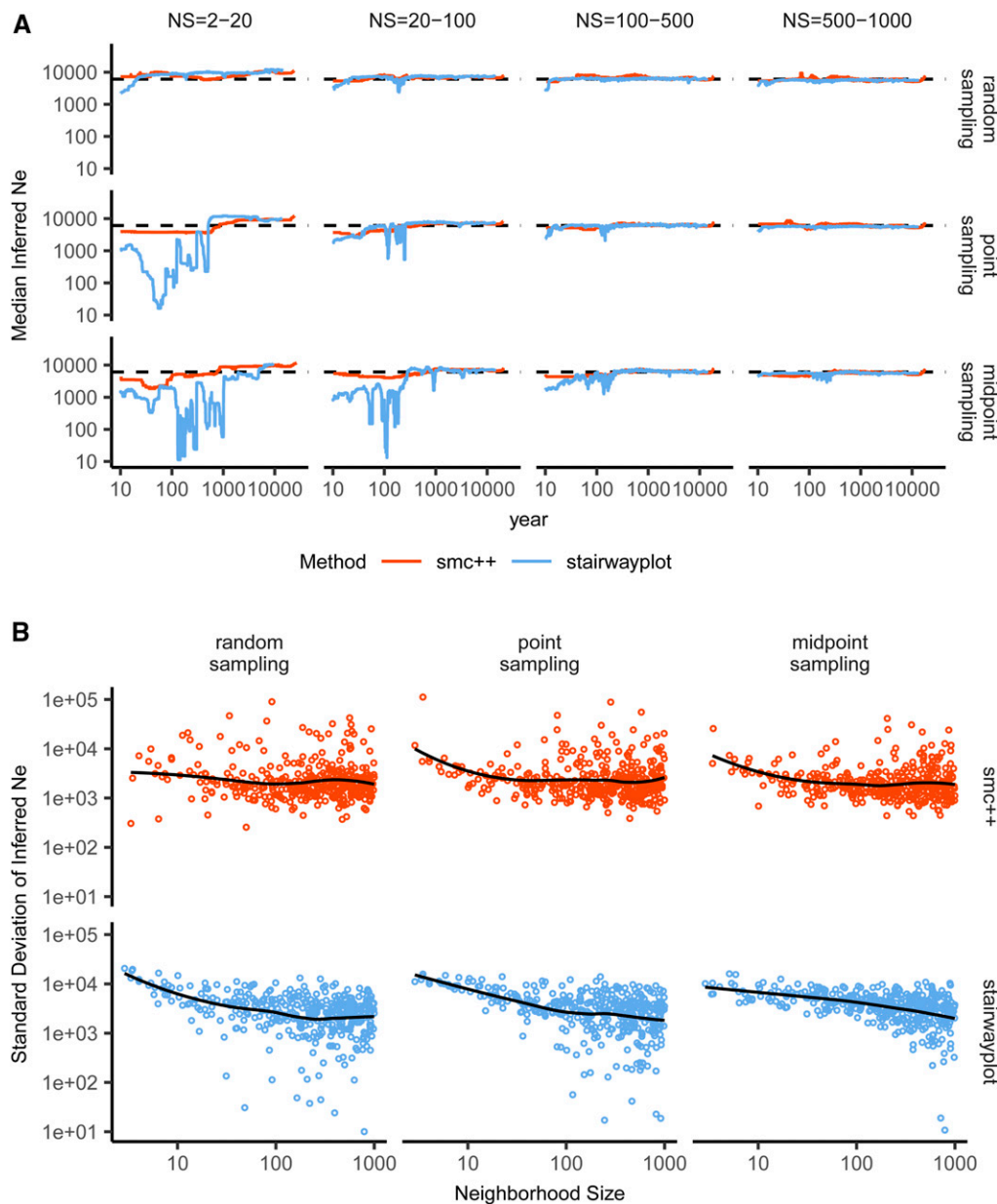
Figure 7 (A) Rolling median inferred N_e trajectories for stairwayplot and smc++ across sampling strategies and NS bins. The dotted line shows the mean N_e of random mating simulations. (B) SD of individual inferred N_e trajectories, by NS and sampling strategy. Black lines are loess curves. Plots including individual model fits are shown in Figure S7. NS, neighborhood size.

2016; Ringbauer *et al.* 2017). Conversely, because haplotype-based measures of demography are particularly sensitive to variation in the underlying genealogy, inference approaches that assume random mating when analyzing the distribution of shared haplotype block lengths are likely to be strongly affected by spatial processes.

Effects of sampling

One of the most important differences between random mating and spatial models is the effect of sampling: in a randomly mating population, the spatial distribution of sampling effort has no effect on estimates of genetic variation (Table S1), but when dispersal is limited, sampling strategy can compound spatial patterns in the underlying genealogy and create pervasive impacts on all downstream genetic analyses [see also

Städler *et al.* (2009)]. In most species, the difficulty of traveling through all parts of a species range and the inefficiency of collecting single individuals at each sampling site means that most studies follow something closest to the point sampling strategy we simulated, in which multiple individuals are sampled from nearby points on the landscape. For example, in ornithology a sample of 10 individuals per species per locality is a common target when collecting for natural history museums. In classical studies of *Drosophila* variation the situation is considerably worse, in which a single orchard might be extensively sampled.

When sampling is clustered at points on a landscape and dispersal is limited, the sampled individuals will be more closely related than a random set of individuals. Average coalescence times of individuals collected at a locality will
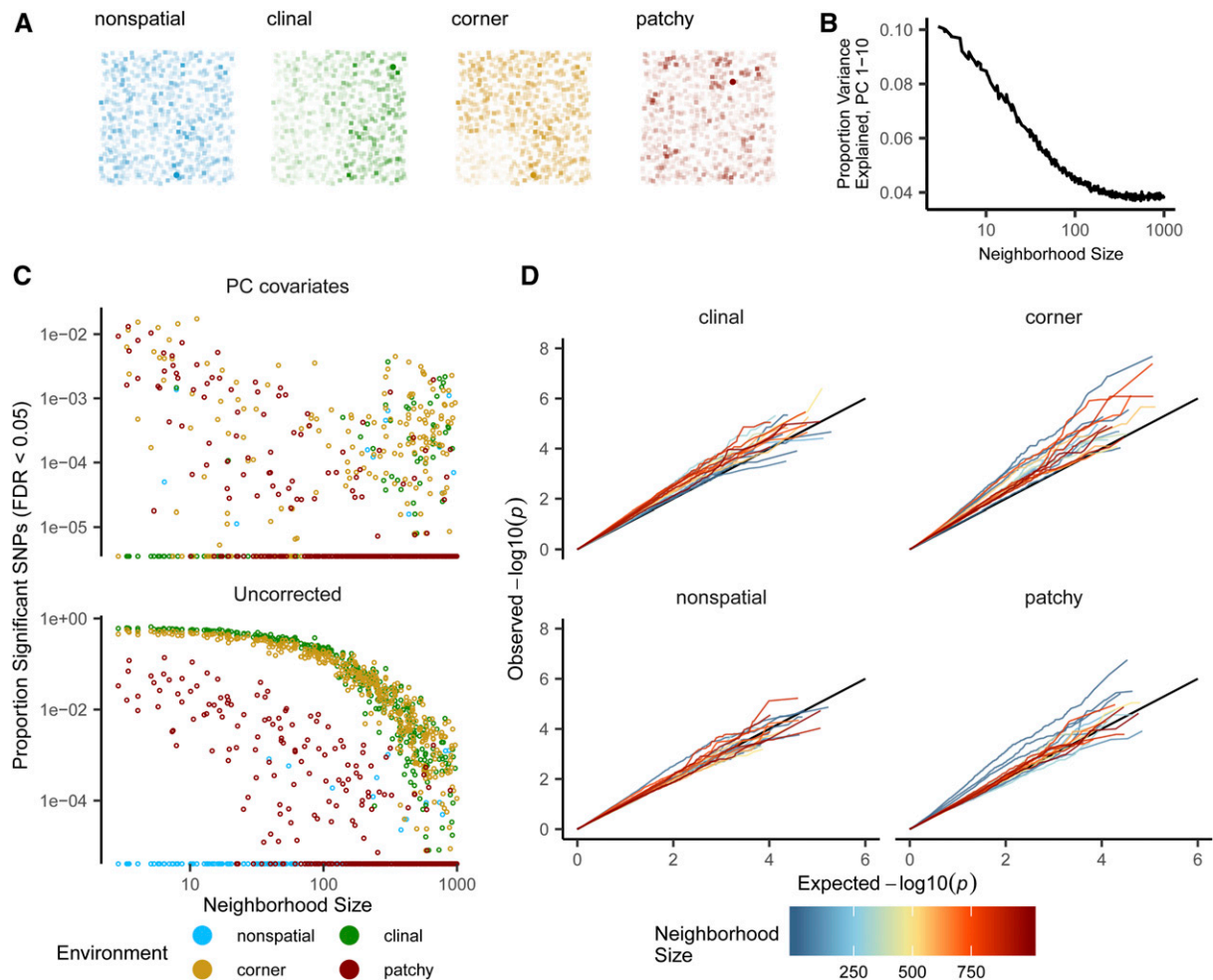
Figure 8 Impacts of spatially varying environments and isolation by distance on linear regression GWAS. Simulated quantitative phenotypes are determined only by an individual's location and the spatial distribution of environmental factors. In (A) we show the phenotypes and locations of sampled individuals under four environmental distributions, with transparency scaled to phenotype. As neighborhood size increases a PCA explains less of the total variation in the data (B). Spatially correlated environmental factors cause false positives at a large proportion of SNPs, which is partially but not entirely corrected by adding the first 10 PC coordinates as covariates (C). Quantile–quantile plots in (D) show inflation of $-\log_{10}(p)$ after PC correction for simulations with spatially structured environments, with line colors showing the neighborhood size of each simulation. FDR, false discovery rate; GWAS, genome-wide association study; PC, principal component; PCA, PC analysis.

then be more recent and branch lengths shorter than expected by analyses assuming random mating. This leads to fewer mutations and recombination events occurring since their last common ancestor, causing a random set of individuals to share longer average IBS tracts and have fewer nucleotide differences. For some data summaries, such as Tajima's D, Watterson's θ, or the correlation coefficient between spatial distance and the count of long haplotype blocks, this can result in large differences in estimates between random and point sampling (Figure 4). Inferring underlying demographic parameters from these summary statistics, unless the spatial locations of the sampled individuals are somehow taken into account, will likely be subject to bias.

We observed the largest sampling effects using midpoint sampling. This model is meant to reflect a bias in sampling effort toward the middle of a species' range. In empirical studies this sampling strategy could arise if, for example,

researchers choose to sample the center of the range and avoid range edges to maximize the probability of locating individuals during a short field season. Because midpoint sampling provides limited spatial resolution, it dramatically reduces the magnitude of observed correlations between spatial and genetic distances. More surprisingly, midpoint sampling also leads to strongly positive Tajima's D and an inflation in the proportion of heterozygous individuals in the sample, similar to the effect of sampling a single deme in an island model as reported in Städler *et al.* (2009). This increase in observed heterozygosity appears to reflect the effects of range edges, which are a fundamental facet of spatial genetic variation. If individuals move randomly in a finite two-dimensional landscape then regions in the middle of the landscape receive migrants from all directions, while those on the edge receive no migrants from at least one direction. The average number of new mutations moving into

the middle of the landscape is then higher than the number moving into regions near the range edge, leading to higher heterozygosity and lower inbreeding coefficients (F_{IS}) away from range edges. Though here we used only a single parameterization of fitness decline at range edges, we believe this is a general property of noninfinite landscapes as it has also been observed in previous studies simulating under lattice models (Neel *et al.* 2013; Shirk and Cushman 2014).

In summary, we recommend that empirical researchers collect individuals from across as much of the species' range as practical, choosing samples separated by a range of spatial scales. Many summary statistics are designed for well-mixed populations, and so provide different insights into genetic variation when applied to different subsets of the population. Applied to a cluster of samples, summary statistics based on segregating sites (*e.g.*, Watterson's θ and Tajima's D), heterozygosity, or the distribution of long haplotype blocks can be expected to depart significantly from what would be obtained from a wider distribution of samples. Comparing the results of analyses conducted on all individuals *vs.* those limited to single individuals per locality can provide an informative contrast. Finally, we wish to point out that the bias toward intermediate allele frequencies that we observe may mean that the importance of linked selection, at least as is gleaned from the SFS, may currently be systematically underestimated.

Demography

Previous studies have found that population structure and nonrandom sampling can create spurious signals of population bottlenecks when attempting to infer demographic history with microsatellite variation, summary statistics, or runs of homozygosity (Ptak and Przeworski 2002; Leblois *et al.* 2006; Städler *et al.* 2009; Chikhi *et al.* 2010; Mazet *et al.* 2015). Here, we found that methods that infer detailed population trajectories through time based on the SFS and patterns of LD across the genome are also subject to this bias, with some combinations of dispersal and sampling strategy systematically inferring deep recent population bottlenecks and overestimating ancient N_e by around a factor of 2. We were surprised to see that both stairwayplot and SMC++ can tolerate relatively strong isolation by distance—*i.e.*, neighborhood sizes of 20—and still perform well when averaging results across multiple simulations (however, note the high amount of between-simulation variance seen in Figure S7). Inference in populations with neighborhood sizes > 20 was relatively unbiased unless samples were concentrated in the middle of the range (Figure 7). Although median demography estimates across many independent simulations were fairly accurate, empirical work has only a single estimate to work with, and individual model fits (Figure S7) suggest that spuriously inferred population size changes and bottlenecks are common, especially at small neighborhood sizes. As we will discuss below, most empirical estimates of neighborhood size, including all estimates for human populations, are large enough that population size trajectories inferred by these approaches should not be strongly affected by spatial biases

created by dispersal in continuous landscapes. In contrast, Mazet *et al.* (2015) found that varying migration rates through time could create strong biases in inferred population trajectories from an *n*-island model with parameters relevant for human history, suggesting that changes in migration rates through time are more likely to drive variation in inferred N_e than isolation by distance.

We found that SMC++ was more robust to the effects of space than stairwayplot, underestimating recent populations by roughly one-half in the worst time periods rather than nearly 10-fold as with stairwayplot. Though this degree of variation in population size is certainly meaningful in an ecological context, it is relatively minor in population genetic terms. Methods directly assessing haplotype structure in phased data examples (*e.g.*, Browning and Browning 2015) are thought to provide increased resolution for recent demographic events, but in this case the error we observed was essentially an accurate reflection of underlying genealogies in which terminal branches are anomalously short. Combined with our analysis of IBS tract length variation (Figure 5) this suggests that haplotype-based methods are likely to be affected by similar biases.

A more worrying pattern was the high level of variance in inferred N_e trajectories for individual model fits using these methods, which was highest in simulations with the smallest neighborhood size (Figure 7 and Figure S7). This suggests that, at a minimum, researchers working with empirical data should replicate analyses multiple times and take a rolling average if model fits are inconsistent across runs. Splitting samples and running replicates on separate subsets, the closest an empirical study can come to our design of averaging the results from multiple simulations, may also alleviate this issue.

Our analysis suggests that many empirical analyses of population size history using methods like SMC++ are robust to error caused by spatial structure within continuous landscapes. Inferences drawn from static SFS-based methods like stairwayplot should be treated with caution when there are signs of isolation by distance in the underlying data (for example, if a regression of F_{ST} against the logarithm of geographic distance has a significantly positive slope), and in particular an inference of population bottlenecks in the last 1000 years should be discounted if sampling is clustered, but estimates of deeper time patterns are likely to be fairly accurate. The biases in the SFS and haplotype structure identified above (see also: Wakeley 1999; Städler *et al.* 2009; Chikhi *et al.* 2010) are apparently small enough that they fall within the range of variability regularly inferred by these approaches, at least on data sets of the size we simulated.

GWAS

Spatial structure is particularly challenging for GWAS, because the effects of dispersal on genetic variation are compounded by spatial variation in the environment (Mathieson and McVean 2012). Spatially restricted mate choice and dispersal causes variation in allele frequencies across the range

of a species. If environmental factors affecting the phenotype of interest also vary over space, then allele frequencies and environmental exposures will covary over space. In this scenario, an uncorrected GWAS will infer genetic associations with a purely environmental phenotype at any site in the genome that is differentiated over space, and the relative degree of bias will be a function of the degree of covariation in allele frequencies and the environment (*i.e.*, Figure 8C, bottom panel). This pattern has been demonstrated in a variety of simulation and empirical contexts (Yu *et al.* 2005; Price *et al.* 2006; Kang *et al.* 2008, 2010; Mathieson and McVean 2012; Bulik-Sullivan *et al.* 2015; Sohail *et al.* 2018 *preprint*; Young *et al.* 2018; Berg *et al.* 2019).

Incorporating PC positions as covariates in a linear-regression GWAS (Price *et al.* 2006) is designed to address this challenge by regressing out a baseline level of average differentiation. In essence, a PC-corrected GWAS asks "what regions of the genome are more associated with this phenotype than the average genome-wide association observed across populations?" In our simulations, we observed that this procedure can fail under a variety of circumstances. If dispersal is limited and environmental variation is clustered in space (*i.e.*, corner or patchy distributions in our simulations), PC positions fail to capture the fine-scale spatial structure required to remove all signals of association. Conversely, as dispersal increases, PCA loses power to describe population structure before spatial mixing breaks down the relationship between genotype and the environment. These effects were observed with all spatially correlated environmental patterns, but were particularly pronounced if environmental effects were concentrated in one region, as was also found by Mathieson and McVean (2012). Though increasing the number of PC axes used in the analysis may reduce the false-positive rate, this may also decrease the power of the test to detect truly causal alleles (Lawson *et al.* 2020).

In this work, we simulated a single chromosome with size roughly comparable to one human chromosome. If we scale the number of false-positive associations identified in our analyses to a GWAS conducted on whole-genome data from humans, we would expect to see several thousand weak false-positive associations after PC corrections in a population with neighborhood sizes up to at least 1000 (which should include values appropriate for many human populations). Notably, very few of the spurious associations we identified would be significant at a conservative Bonferroni-adjusted *P*-value cut-off (see Figure S8). This suggests that GWAS focused on finding strongly associated alleles for traits controlled by a limited number of variants in the genome are likely robust to the impacts of continuous spatial structure. However, methods that analyze the combined effects of thousands or millions of weakly associated variants, such as polygenic risk scores (Wray *et al.* 2007; International Schizophrenia Consortium *et al.* 2009), are likely to be affected by subtle population structure. Indeed, as recently identified in studies of genotype associations for human height in Europe (Sohail *et al.* 2018 *preprint*; Berg *et al.* 2019), PC regression GWAS in modern human populations do include residual signals of population structure in large-scale analyses of polygenic traits. In addition to errors associated with varying patterns of LD and allele frequency among populations, the confounding of environmental and genetic effects on phenotypes introduced by population structure is expected to lead to low predictive power when polygenic scores are generated for populations outside the original GWAS cohort, as was shown in a recent study finding lower polygenic score predictive power outside European populations (Martin *et al.* 2019).

In summary, spatial covariation in population structure and the environment confounds the interpretation of GWAS *P*-values, and correction using PCs is insufficient to fully separate these signals for polygenic traits under a variety of environmental and population parameter regimes. Other GWAS methods such as mixed models (Kang *et al.* 2008) may be less sensitive to this confounding, but there is no obvious reason that this should be so. One approach to estimating the degree of bias in GWAS caused by population structure is LD score regression (Bulik-Sullivan *et al.* 2015). Though this approach appears to work well in practice, its interpretation is not always straightforward and it is likely biased by the presence of linked selection (Berg *et al.* 2019). In addition, we observed that in many cases the false-positive SNPs we identified appeared to be concentrated in LD peaks similar to those expected from truly causal sites (Figure S8), which may confound LD score regression.

We suggest a straightforward alternative for species in which the primary axes of population differentiation are associated with geography (note this is likely not the case for some modern human populations): run a GWAS with spatial coordinates as phenotypes and check for *P*-value inflation or significant associations. If significant associations with sample locality are observed after correcting for population structure, the method is sensitive to false positives induced by spatial structure. This is essentially the approach taken in our clinal model (though we add normally distributed noise to our phenotypes). This approach was recently taken with polygenic scores for UK Biobank samples in Haworth *et al.* (2019), finding that scores are correlated with birth location even in this relatively homogenous sample. Of course, it is possible that genotypes indirectly affect individual locations by adjusting organismal fitness and thus habitat selection across spatially varying environments, but we believe that this hypothesis should be tested against a null of stratification bias inflation rather than accepted as true based on GWAS results.

Where are natural populations on this spectrum?

For how much of the tree of life do spatial patterns circumscribe genomic variation? In Table 1, we gathered estimates of neighborhood size from a range of organisms to get an idea of how strongly local geographic dispersal affects patterns of variation. This is an imperfect measure: some aspects of genetic variation are most strongly determined by neighborhood size (Wright 1946), others (*e.g.*, number of

segregating sites) by global N_e, or the ratio of the two. In addition, definitions of population density in genetic *vs.* ecological studies may lead to varying estimates of neighborhood size for a given species, and these empirical examples may be biased toward small-neighborhood species because few studies have quantified neighborhood size in species with very high dispersal or population density.

However, from the available data we find that neighborhood sizes in the range we simulated are fairly common across a range of taxa. At the extreme low end of empirical neighborhood size estimates we see some flowering plants, large mammals, and colonial insects like ants with neighborhood sizes less than roughly 100. Species such as this have neighborhood size estimates small enough that spatial processes are likely to strongly influence inference. These include some human populations such as the Gainj- and Kalam-speaking people of Papua New Guinea, in which the estimated neighborhood sizes in Rousset (1997) range from 40 to 410 depending on the method of estimation. Many more species occur in a middle range of neighborhood sizes between 100 and 1000, a range in which spatial processes play a minor role in our analyses under random spatial sampling but are important when sampling of individuals in space is clustered. Surprisingly, even some flying insects with huge census population sizes fall in this group, including fruit flies (*Drosophila melanogaster*) and mosquitoes (*Aedes aegypti*). Last, many species likely have neighborhood sizes much larger than we simulated, including the recent ancestors of modern humans in northeastern Europe (Ringbauer *et al.* 2017). For these species, demographic inference and summary statistics are likely to reflect minimal bias from spatial effects as long as dispersal is truly continuous across the landscape. While that is so, we caution that association studies in which the effects of population structure are confounded with spatial variation in the environment are still sensitive to dispersal even at these large neighborhood sizes.

Other demographic models

Any simulation of a population of reproducing organisms requires some kind of control on population sizes, or else the population will either die out or grow very large after a sufficiently long period of time. The usual choice of population regulation for population genetics—a constant size, as in the Wright–Fisher model—implies biologically unrealistic interactions between geographically distant parts of the species range. Our choice to regulate population size by including a local density-dependent control on mortality is only one of many possible ways to do this. We could have instead regulated fecundity, or recruitment, or both; this general class of models is sometimes referred to as the "Bolker–Pacala model" (Bolker and Pacala 1997). It is not currently clear how much different choices of demographic parameters, or of functional forms for the regulation, might quantitatively affect our results, although the general predictions should be robust to similar forms of regulation. As is usual in population genetics, the populations are entirely *intrinsically* regulated.

Alternatively, population size could be regulated by interactions with other species (*e.g.*, a Lotka–Volterra model) or extrinsically specified by local resource availability (*e.g.*, by food or nest site availability). Indeed, our model could be interpreted as a caricature of such a model: as local density increases, good habitat is increasingly occupied, pushing individuals into more marginal habitat and increasing their mortality. Many such models should behave similarly to ours, but others (especially those with local population cycling) may differ dramatically.

Population genetic simulations often use grids of discrete demes, which are assumed to approximate continuous space. However, there are theoretical reasons to expect that increasingly fine grids of discrete demes do not approach the continuous model (Barton *et al.* 2002). If continuous space can be approximated by a limit of discrete models, this should be true regardless of the precise details of the discrete model. Although we carefully chose parameters to match our continuous models, we found that some aspects of genetic variation diverged from the continuous case as the discretization got finer. This suggests that these models do not converge in the limit. However, many populations may indeed be well modeled as a series of discrete, randomly mating demes if, for example, suitable habitats are patchily distributed across the landscape. There is a clear need for greater exploration of the consequences for population genetics of ecologically realistic population models.

Future directions and limitations

As we have shown, a large number of population genetic summary statistics contain information about spatial population processes. We imagine that combinations of such summaries might be sufficient for the construction of supervised machine learning regressors (*e.g.*, Schrider and Kern 2018) for the accurate estimation of dispersal from genetic data. Indeed, Ashander *et al.* (2018 *preprint*) found that inverse interpolation on a vector of summary statistics provided a powerful method of estimating dispersal distances. Expanding this approach to include the haplotype-based summary statistics studied here and applying machine learning regressors built for general inference of nonlinear relationships from high-dimensional data may allow precise estimation of spatial parameters under a range of complex models.

One facet of spatial variation that we did not address in this study is the confounding of dispersal and population density implicit in the definition of Wright's neighborhood size. Our simulations were run under constant densities, but Guindon *et al.* (2016) and Ringbauer *et al.* (2017) have shown that these parameters are identifiable under some continuous models. Similarly, though the scaling effects of dispersal we show in Figure 4 should occur in populations of any total size, other aspects such as the number of segregating sites are also likely affected by the total landscape size (and so total census size). Indeed, our finding that stepping-stone and continuous-space models match in only certain aspects of genetic variation (Figure A1) shows that qualitatively similar models

can produce different results dependent on the specific parameterizations used. While we believe our continuous model is a more appropriate depiction of many species' demographies than lattice models, it is likely that some populations and breeding systems do more closely resemble a series of interconnected random mating populations. As with all population models, the best approximation for any empirical system will depend on the natural history of the species in question. Much additional work remains to be done to better understand how life history, range size, and habitat geometry interact to shape genetic variation in continuous space, which we leave to future studies.

Though our simulation allows incorporation of realistic demographic and spatial processes, it is inevitably limited by the computational burden of tracking tens or hundreds of thousands of individuals in every generation. In particular, computations required for mate selection and spatial competition scale approximately with the product of the total census size and the neighborhood size, and so increase rapidly for large populations and dispersal distances. The reverse-time spatial Λ-Fleming–Viot model described by Barton *et al.* (2010) and implemented by Kelleher *et al.* (2014) allows exploration of larger population and landscape sizes, but the precise connection of these models to forward-time demography is not yet clear. Alternatively, implementation of parallelized calculations may allow progress with forward-time simulations.

Finally, we believe that the difficulties in correcting for population structure in continuous populations using PCA or similar decompositions is a difficult issue, well worth considering on its own. How can we best avoid spurious correlations while correlating genetic and phenotypic variation without underpowering the methods? Perhaps optimistically, we posit that process-driven descriptions of ancestry and/or more generalized unsupervised methods may be able to better account for carrying out this task.

Acknowledgments

Literature Cited

Aguillon, S. M., J. W. Fitzpatrick, R. Bowman, S. J. Schoech, A. G. Clark *et al.*, 2017 Deconstructing isolation-by-distance: the genomic consequences of limited dispersal. PLoS Genet. 13: e1006911. https://doi.org/10.1371/journal.pgen.1006911

Al-Asadi, H., D. Petkova, M. Stephens, and J. Novembre, 2019 Estimating recent migration and population-size surfaces. PLoS Genet. 15: e1007908. https://doi.org/10.1371/journal.pgen.1007908

Allee, W. C., O. Park, A. E. Emerson, T. Park, K. P. Schmidt *et al.*, 1949 *Principles of Animal Ecology. Technical Report*. Saunders Company, Philadelphia, PA.

Antlfinger, A. E., 1982 Genetic neighborhood structure of the salt marsh composite, *Borrichia frutescens*. J. Hered. 73: 128–132. https://doi.org/10.1093/oxfordjournals.jhered.a109595

Antolin, M. F., B. V. Horne, M. D. Berger, Jr., A. K. Holloway, J. L. Roach *et al.*, 2001 Effective population size and genetic structure of a piute ground squirrel (*Spermophilus mollis*) population. Can. J. Zool. 79: 26–34. https://doi.org/10.1139/z00-170

Antonovics, J., and D. A. Levin, 1980 The ecological and genetic consequences of density-dependent regulation in plants. Annu. Rev. Ecol. Syst. 11: 411–452. https://doi.org/10.1146/annurev.es.11.110180.002211

Ashander, J., P. Ralph, E. McCartney-Melstad, and H. B. Shaffer, 2018 Demographic inference in a spatially-explicit ecological model from genomic data: a proof of concept for the Mojave Desert tortoise. bioRxiv. (Preprint posted June 23, 2018).https://doi.org/10.1101/354530

Baharian, S., M. Barakatt, C. R. Gignoux, S. Shringarpure, J. Errington *et al.*, 2016 The great migration and African-American genomic diversity. PLoS Genet. 12: e1006059. https://doi.org/10.1371/journal.pgen.1006059

Barton, N. H., F. Depaulis, and A. M. Etheridge, 2002 Neutral evolution in spatially continuous populations. Theor. Popul. Biol. 61: 31–48. https://doi.org/10.1006/tpbi.2001.1557

Barton, N. H., J. Kelleher, and A. M. Etheridge, 2010 A new model for extinction and recolonization in two dimensions: quantifying phylogeography. Evolution 64: 2701–2715. https://doi.org/10.1111/j.1558-5646.2010.01019.x

Benjamini, Y., and D. Yekutieli, 2001 The control of the false discovery rate in multiple testing under dependency. Ann. Stat. 29: 1165–1188.

Berg, E. E., and J. L. Hamrick, 1995 Fine-scale genetic structure of a turkey oak forest. Evolution 49: 110–120. https://doi.org/10.1111/j.1558-5646.1995.tb05963.x

Berg, J. J., A. Harpak, N. Sinnott-Armstrong, A. M. Joergensen, H. Mostafavi *et al.*, 2019 Reduced signal for polygenic adaptation of height in UK Biobank. Elife 8: e39725. https://doi.org/10.7554/eLife.39725

Bolker, B., and S. W. Pacala, 1997 Using moment equations to understand stochastically driven spatial pattern formation in ecological systems. Theor. Popul. Biol. 52: 179–197. https://doi.org/10.1006/tpbi.1997.1331

Bolker, B. M., S. W. Pacala, and C. Neuhauser, 2003 Spatial dynamics in model plant communities: what do we really know? Am. Nat. 162: 135–148. https://doi.org/10.1086/376575

Browning, S. R., and B. L. Browning, 2015 Accurate non-parametric estimation of recent effective population size from segments of identity by descent. Am. J. Hum. Genet. 97: 404–418. https://doi.org/10.1016/j.ajhg.2015.07.012

Bulik-Sullivan, B. K., P.-R. Loh, H. K. Finucane, S. Ripke, J. Yang *et al.*, 2015 LD score regression distinguishes confounding from polygenicity in genome-wide association studies. Nat. Genet. 47: 291–295. https://doi.org/10.1038/ng.3211

Campbell, D. R., and J. L. Dooley, 1992 The spatial scale of genetic differentiation in a hummingbird-pollinated plant: comparison with models of isolation by distance. Am. Nat. 139: 735–748. https://doi.org/10.1086/285355

Champer, J., I. Kim, S. E. Champer, A. G. Clark, and P. W. Messer, 2019 Suppression gene drive in continuous space can result in unstable persistence of both drive and wild-type alleles. bioRxiv. (Preprint posted September 14, 2019).https://doi.org/10.1101/769810

Chapman, N. H., and E. A. Thompson, 2002 The effect of population history on the lengths of ancestral chromosome segments. Genetics 162: 449–458.

Chikhi, L., V. C. Sousa, P. Luisi, B. Goossens, and M. A. Beaumont, 2010   The confounding effects of population structure, genetic diversity and the sampling scheme on the detection and quantification of population size changes. Genetics 186: 983–995. https://doi.org/10.1534/genetics.110.118661

Crawley, M. J., 1990   The population dynamics of plants. Philos. Trans. R. Soc. Lond. B Biol. Sci. 330: 125–140. https://doi.org/10.1098/rstb.1990.0187

Durrett, R., and S. Levin, 1994   The importance of being discrete (and spatial). Theor. Popul. Biol. 46: 363–394. https://doi.org/10.1006/tpbi.1994.1032

Eguiarte, L. E., A. Búrquez, J. Rodríguez, M. Martínez-Ramos, J. Sarukhán et al., 1993   Direct and indirect estimates of neighborhood and effective population size in a tropical palm, Astrocaryum mexicanum. Evolution 47: 75–87. https://doi.org/10.1111/j.1558-5646.1993.tb01200.x

Epperson, B. K., 2003   Geographical Genetics. Princeton University Press, Princeton, NJ. https://doi.org/10.1515/9781400835621

Felsenstein, J., 1975   A pain in the torus: some difficulties with models of isolation by distance. Am. Nat. 109: 359–368. https://doi.org/10.1086/283003

Fournier, N., and S. Méléard, 2004   A microscopic probabilistic description of a locally regulated population and macroscopic approximations. Ann. Appl. Probab. 14: 1880–1919. https://doi.org/10.1214/105051604000000882

Fox, J., and S. Weisberg, 2011   An R Companion to Applied Regression, Ed. 2. Sage, Thousand Oaks, CA.

Garcia, J., and C. Quintana-Domeque, 2007   The evolution of adult height in Europe: a brief note. Econ. Hum. Biol. 5: 340–349. https://doi.org/10.1016/j.ehb.2007.02.002

Garud, N. R., P. W. Messer, E. O. Buzbas, and D. A. Petrov, 2015   Recent selective sweeps in North American Drosophila melanogaster show signatures of soft sweeps. PLoS Genet. 11: e1005004. https://doi.org/10.1371/journal.pgen.1005004

Griffiths, R., and S. Tavaré, 1999   The ages of mutations in gene trees. Ann. Appl. Probab. 9: 567–590. https://doi.org/10.1214/aoap/1029962804

Guindon, S., H. Guo, and D. Welch, 2016   Demographic inference under the coalescent in a spatial continuum. Theor. Popul. Biol. 111: 43–50. https://doi.org/10.1016/j.tpb.2016.05.002

Haller, B. C., and P. W. Messer, 2019   SLiM 3: forward genetic simulations beyond the Wright–Fisher model. Mol. Biol. Evol. 36: 632–637. https://doi.org/10.1093/molbev/msy228

Haller, B. C., J. Galloway, J. Kelleher, P. W. Messer, and P. L. Ralph, 2019   Tree-sequence recording in SLiM opens new horizons for forward-time simulation of whole genomes. Mol. Ecol. Resour. 19: 552–566. https://doi.org/10.1111/1755-0998.12968

Harris, K., and R. Nielsen, 2013   Inferring demographic history from a spectrum of shared haplotype lengths. PLoS Genet. 9: e1003521. https://doi.org/10.1371/journal.pgen.1003521

Haworth, S., R. Mitchell, L. Corbin, K. H. Wade, T. Dudding et al., 2019   Apparent latent structure within the UK Biobank sample has implications for epidemiological analysis. Nat. Commun. 10: 333. https://doi.org/10.1038/s41467-018-08219-1

Huillet, T., and M. Möhle, 2013   On the extended Moran model and its relation to coalescents with multiple collisions. Theor. Popul. Biol. 87: 5–14. https://doi.org/10.1016/j.tpb.2011.09.004

International Schizophrenia Consortium, Purcell, S. M., N. R. Wray, J. L. Stone, P. M. Visscher, et al., 2009   Common polygenic variation contributes to risk of schizophrenia and bipolar disorder. Nature 460: 748–752. https://doi.org/10.1038/nature08185

Jackson, N. D., and L. Fahrig, 2014   Landscape context affects genetic diversity at a much larger spatial extent than population abundance. Ecology 95: 871–881. https://doi.org/10.1890/13-0388.1

Jasper, M., T. Schmidt, N. Ahmad, S. Sinkins, and A. Hoffmann, 2019   A genomic approach to inferring kinship reveals limited intergenerational dispersal in the yellow fever mosquito. Mol. Ecol. Resour. 19: 1254–1264.

Jay, F., P. Sjödin, M. Jakobsson, and M. G. Blum, 2012   Anisotropic isolation by distance: the main orientations of human genetic differentiation. Mol. Biol. Evol. 30: 513–525. https://doi.org/10.1093/molbev/mss259

Kang, H. M., N. A. Zaitlen, C. M. Wade, A. Kirby, D. Heckerman et al., 2008   Efficient control of population structure in model organism association mapping. Genetics 178: 1709–1723. https://doi.org/10.1534/genetics.107.080101

Kang, H. M., J. H. Sul, S. K. Service, N. A. Zaitlen, S.-y. Kong et al., 2010   Variance component model to account for sample structure in genome-wide association studies. Nat. Genet. 42: 348–354. https://doi.org/10.1038/ng.548

Kelleher, J., A. Etheridge, and N. Barton, 2014   Coalescent simulation in continuous space: algorithms for large neighbourhood size. Theor. Popul. Biol. 95: 13–23. https://doi.org/10.1016/j.tpb.2014.05.001

Kelleher, J., A. M. Etheridge, and G. McVean, 2016   Efficient coalescent simulation and genealogical analysis for large sample sizes. PLoS Comput. Biol. 12: e1004842. https://doi.org/10.1371/journal.pcbi.1004842

Kelleher, J., K. R. Thornton, J. Ashander, and P. L. Ralph, 2018   Efficient pedigree recording for fast population genetics simulation. PLoS Comput. Biol. 14: e1006581. https://doi.org/10.1371/journal.pcbi.1006581

Kerster, H. W., 1964   Neighborhood size in the rusty lizard, Sceloporus olivaceus. Evolution 18: 445–457. https://doi.org/10.1111/j.1558-5646.1964.tb01621.x

Kingman, J., 1982   The coalescent. Stochastic Process. Appl. 13: 235–248. https://doi.org/10.1016/0304-4149(82)90011-4

Law, R., D. J. Murrell, and U. Dieckmann, 2003   Population growth in space and time: spatial logistic equations. Ecology 84: 252–262. https://doi.org/10.1890/0012-9658(2003)084-[0252:PGISAT]2.0.CO;2

Lawson, D. J., N. M. Davies, S. Haworth, B. Ashraf, L. Howe et al., 2020   Is population structure in the genetic biobank era irrelevant, a challenge, or an opportunity? Hum. Genet. 139: 23–41 (erratum: Hum. Genet. 139: 43–44). https://doi.org/10.1007/s00439-019-02014-8

Leblois, R., A. Estoup, and R. Streiff, 2006   Genetics of recent habitat contraction and reduction in population size: does isolation by distance matter? Mol. Ecol. 15: 3601–3615. https://doi.org/10.1111/j.1365-294X.2006.03046.x

Liu, X., and Y.-X. Fu, 2015   Exploring population size changes using SNP frequency spectra. Nat. Genet. 47: 555–559 (erratum: Nat Genet. 47: 1099). https://doi.org/10.1038/ng.3254

Lloyd, M., 1967   'Mean crowding'. J. Anim. Ecol. 36: 1–30. https://doi.org/10.2307/3012

Lundgren, E., and P. L. Ralph, 2019   Are populations like a circuit? Comparing isolation by resistance to a new coalescent-based method. Mol. Ecol. Resour. 19: 1388–1406. https://doi.org/10.1111/1755-0998.13035

Martin, A. R., M. Kanai, Y. Kamatani, Y. Okada, B. M. Neale et al., 2019   Clinical use of current polygenic risk scores may exacerbate health disparities. Nat. Genet. 51: 584–591. https://doi.org/10.1038/s41588-019-0379-x

Maruyama, T., 1972   Rate of decrease of genetic variability in a two-dimensional continuous population of finite size. Genetics 70: 639–651.

Mathieson, I., and G. McVean, 2012   Differential confounding of rare and common variants in spatially structured populations. Nat. Genet. 44: 243–246. https://doi.org/10.1038/ng.1074

Mazet, O., W. Rodríguez, S. Grusea, S. Boitard, and L. Chikhi, 2015   On the importance of being structured: instantaneous coalescence rates and human evolution--lessons for ancestral

population size inference? Heredity (Edinb.) 116: 362–371. https://doi.org/10.1038/hdy.2015.104

[11] Miles, A., and N. Harding, 2017 cggh/scikit-allel: v1.1.8.

Neel, M. C., K. McKelvey, N. Ryman, M. W. Lloyd, R. Short Bull *et al.*, 2013 Estimation of effective population size in continuously distributed populations: there goes the neighborhood. Heredity (Edinb.) 111: 189–199. https://doi.org/10.1038/hdy.2013.37

Novembre, J., and M. Slatkin, 2009 Likelihood-based inference in isolation-by-distance models using the spatial distribution of low-frequency alleles. Evolution 63: 2914–2925. https://doi.org/10.1111/j.1558-5646.2009.00775.x

Pamilo, P., 1983 Genetic differentiation within subdivided populations of formica ants. Evolution 37: 1010–1022. https://doi.org/10.1111/j.1558-5646.1983.tb05629.x

Patterson, N., A. L. Price, and D. Reich, 2006 Population structure and eigenanalysis. PLoS Genet. 2: e190. https://doi.org/10.1371/journal.pgen.0020190

Petkova, D., J. Novembre, and M. Stephens, 2015 Visualizing spatial population structure with estimated effective migration surfaces. Nat. Genet. 48: 94–100. https://doi.org/10.1038/ng.3464

Price, A. L., N. J. Patterson, R. M. Plenge, M. E. Weinblatt, N. A. Shadick *et al.*, 2006 Principal components analysis corrects for stratification in genome-wide association studies. Nat. Genet. 38: 904–909. https://doi.org/10.1038/ng1847

Pritchard, J. K., M. Stephens, and P. Donnelly, 2000 Inference of population structure using multilocus genotype data. Genetics 155: 945–959.

Ptak, S. E., and M. Przeworski, 2002 Evidence for population growth in humans is confounded by fine-scale population structure. Trends Genet. 18: 559–563. https://doi.org/10.1016/S0168-9525(02)02781-6

Purcell, S., B. Neale, K. Todd-Brown, L. Thomas, M. A. Ferreira *et al.*, 2007 Plink: a tool set for whole-genome association and population-based linkage analyses. Am. J. Hum. Genet. 81: 559–575. https://doi.org/10.1086/519795

Ralph, P., and G. Coop, 2013 The geography of recent genetic ancestry across Europe. PLoS Biol. 11: e1001555. https://doi.org/10.1371/journal.pbio.1001555

[12] Ralph, P., J. Kelleher, J. Galloway, and J. Ashander, 2019a pyslim.

Ralph, P., K. Thornton, and J. Kelleher, 2019b Efficiently summarizing relationships in large samples: a general duality between statistics of genealogies and genomes. bioRxiv. (Preprint posted September 23, 2019).https://doi.org/10.1101/779132

R Core Team, 2018 *R: A Language and Environment for Statistical Computing*. R Foundation for Statistical Computing, Vienna.

Ringbauer, H., G. Coop, and N. H. Barton, 2017 Inferring recent demography from isolation by distance of long shared sequence blocks. Genetics 205: 1335–1351. https://doi.org/10.1534/genetics.116.196220

Robledo-Arnuncio, J. J., and F. Rousset, 2010 Isolation by distance in a continuous population under stochastic demographic fluctuations. J. Evol. Biol. 23: 53–71. https://doi.org/10.1111/j.1420-9101.2009.01860.x

Rossine, F. W. S., 2014 Espaço e diversificação: uma perspectiva teórica. Master's Dissertation, University of São Paulo, São Paulo. 10.11606/D.41.2014.tde-22092014-112838https://doi.org/10.11606/D.41.2014.tde-22092014-112838

Rousset, F., 1997 Genetic differentiation and estimation of gene flow from F-statistics under isolation by distance. Genetics 145: 1219–1228.

Rousset, F., and R. Leblois, 2011 Likelihood-based inferences under isolation by distance: two-dimensional habitats and confidence intervals. Mol. Biol. Evol. 29: 957–973. https://doi.org/10.1093/molbev/msr262

Sawyer, S., 1977 On the past history of an allele now known to have frequency p. J. Appl. Probab. 14: 439–450. https://doi.org/10.2307/3213447

Schiffels, S., and R. Durbin, 2014 Inferring human population size and separation history from multiple genome sequences. Nat. Genet. 46: 919–925. https://doi.org/10.1038/ng.3015

Schrider, D. R., and A. D. Kern, 2018 Supervised machine learning for population genetics: a new paradigm. Trends Genet. 34: 301–312. https://doi.org/10.1016/j.tig.2017.12.005

Sharbel, T. F., B. Haubold, and T. Mitchell-Olds, 2000 Genetic isolation by distance in *Arabidopsis thaliana*: biogeography and postglacial colonization of Europe. Mol. Ecol. 9: 2109–2118. https://doi.org/10.1046/j.1365-294X.2000.01122.x

Sheehan, S., K. Harris, and Y. S. Song, 2013 Estimating variable effective population sizes from multiple genomes: a sequentially Markov conditional sampling distribution approach. Genetics 194: 647–662. https://doi.org/10.1534/genetics.112.149096

Shirk, A. J., and S. A. Cushman, 2014 Spatially-explicit estimation of Wright's neighborhood size in continuous populations. Front. Ecol. Evol. 2: 62. https://doi.org/10.3389/fevo.2014.00062

Slatkin, M., and N. H. Barton, 1989 A comparison of three indirect methods for estimating average levels of gene flow. Evolution 43: 1349–1368. https://doi.org/10.1111/j.1558-5646.1989.tb02587.x

Sohail, M., R. M. Maier, A. Ganna, A. Bloemendal, A. R. Martin *et al.*, 2018 Signals of polygenic adaptation on height have been overestimated due to uncorrected population structure in genome-wide association studies. bioRxiv. (Preprint posted June 25, 2018).https://doi.org/10.1101/355057

Städler, T., B. Haubold, C. Merino, W. Stephan, and P. Pfaffelhuber, 2009 The impact of sampling schemes on the site frequency spectrum in nonequilibrium subdivided populations. Genetics 182: 205–216. https://doi.org/10.1534/genetics.108.094904

St. Onge, K. R., A. E. Palmé, S. I. Wright, and M. Lascoux, 2012 Impact of sampling schemes on demographic inference: an empirical study in two species with different mating systems and demographic histories. G3 (Bethesda) 2: 803–814.

Tajima, F., 1989 Statistical method for testing the neutral mutation hypothesis by DNA polymorphism. Genetics 123: 585–595.

Terhorst, J., J. A. Kamm, and Y. S. Song, 2016 Robust and scalable inference of population history from hundreds of unphased whole genomes. Nat. Genet. 49: 303–309. https://doi.org/10.1038/ng.3748

Turchin, M. C., C. W. Chiang, C. D. Palmer, S. Sankararaman, D. Reich *et al.*, 2012 Evidence of widespread selection on standing variation in Europe at height-associated SNPs. Nat. Genet. 44: 1015–1019. https://doi.org/10.1038/ng.2368

Wahlund, S., 1928 Zusammensetzung von populationen und korrelationserscheinungen vom standpunkt der vererbungslehre aus betrachtet. Hereditas 11: 65–106. https://doi.org/10.1111/j.1601-5223.1928.tb02483.x

Wakeley, J., 1999 Nonequilibrium migration in human history. Genetics 153: 1863–1871.

Wakeley, J., 2009 *Coalescent Theory, an Introduction*. Roberts and Company, Greenwood Village, CO.

Wakeley, J., and T. Takahashi, 2003 Gene genealogies when the sample size exceeds the effective size of the population. Mol. Biol. Evol. 20: 208–213. https://doi.org/10.1093/molbev/msg024

Wickham, H., 2016 ggplot2: Elegant Graphics for Data Analysis. Springer-Verlag, New York.

Wilke, C. O., 2019 cowplot: streamlined plot theme and plot annotations for 'ggplot2'. R package version 0.9.4. [13]

Wilkins, J. F., 2004 A separation-of-timescales approach to the coalescent in a continuous population. Genetics 168: 2227–2244. https://doi.org/10.1534/genetics.103.022830

Wilkins, J. F., and J. Wakeley, 2002 The coalescent in a continuous, finite, linear population. Genetics 161: 873–888.

Wray, N. R., M. E. Goddard, and P. M. Visscher, 2007 Prediction of individual genetic risk to disease from genome-wide association studies. Genome Res. 17: 1520–1528. https://doi.org/10.1101/gr.6665407

Wright, S., 1931 Evolution in Mendelian populations. Genetics 16: 97.

Wright, S., 1943 Isolation by distance. Genetics 28: 114–138.

Wright, S., 1946 Isolation by distance under diverse systems of mating. Genetics 31: 336.

Young, A. I., M. L. Frigge, D. F. Gudbjartsson, G. Thorleifsson, G. Bjornsdottir et al., 2018 Relatedness disequilibrium regression estimates heritability without environmental bias. Nat. Genet. 50: 1304–1310. https://doi.org/10.1038/s41588-018-0178-9

Young, H. J., 1988 Neighborhood size in a beetle pollinated tropical aroid: effects of low density and asynchronous flowering. Oecologia 76: 461–466. https://doi.org/10.1007/BF00377043

Yu, J., G. Pressoir, W. H. Briggs, I. Vroh Bi, M. Yamasaki et al., 2005 A unified mixed-model method for association mapping that accounts for multiple levels of relatedness. Nat. Genet. 38: 203–208. https://doi.org/10.1038/ng1702

Zähle, I., J. T. Cox, and R. Durrett, 2005 The stepping stone model. II. Genealogies and the infinite sites model. Ann. Appl. Probab. 15: 671–699. https://doi.org/10.1214/105051604000000701

Communicating editor: J. Novembre

Appendix

Comparisons with Stepping-Stone Models

We also compared our model results to a regular grid of discrete populations, which is commonly used as an approximation of continuous geography. An important reason that this approximation is often made is that it allows more efficient, coalescent simulations; we implemented these using msprime (Kelleher *et al.*, 2016). In this class of model, we imagine an $n \times n$ grid of populations exchanging migrants with neighboring populations at rate m. If these models are good approximations of the continuous case we expect that results will converge as $n \to \infty$ (while scaling m appropriately and keeping total population size fixed), so we ran simulations while varying n from 5 to 50 (Table A1). To compare with continuous models, we first distributed the same effective number of individuals across the landscape as in our continuous-space simulations ($\sim$6100, estimated from θ_π of random mating continuous-space simulations). We then approximated the mean per generation dispersal distance σ given a total landscape width W as the product of the probability of an individual being a migrant and the distance traveled by migrants: $\sigma = 4m(W/n)$. This means that m in different simulations with the same σ scales with $\sqrt{n}$. We ran 500 simulations for each value of n while sampling σ from $U(0.2, 4)$. We then randomly selected 60 diploid individuals from each simulation (approximating diploidy by combining pairs of chromosomes with contiguous indices within demes) and calculated a set of six summary statistics using the scripts described in the summary statistics portion of the main text.

In general, we find that many of the qualitative trends are similar among continuous and stepping-stone models and that, at low neighborhood sizes, many (but not all) statistics from stepping-stone models approach the continuous model as the resolution of the grid increases. For example, θ_π is lower in stepping-stone models at low neighborhood sizes (*i.e.*, low m), but increases to approach the continuous case as the resolution of the landscape increases. Similar patterns are observed for observed heterozygosity. However, θ_W behaves differently, showing a nonmonotonic relationship with grid resolution. This results in an increasingly positive Tajima's D in grid simulations at small neighborhood sizes, to a much greater extent than seen in a continuous model. In contrast to θ_π, increasing the resolution of the grid causes Tajima's D to deviate *more* from what is seen in the continuous model. Similarly, although F_{IS} approaches the continuous case as the resolution of the grid increases at very small neighborhood sizes, at intermediate neighborhood sizes the continuous case best matches intermediate grid resolutions.

These differences relative to our continuous model mainly reflect two shortcomings of the reverse-time stepping-stone model. If we simulate a coarse grid with relatively large populations in each deme, we cannot accurately capture the dynamics of small neighborhood sizes because mating within each deme remains random regardless of the migration rate connecting demes. This likely explains the trends in θ_π, observed heterozygosity, and F_{IS}. However, increasing the number of demes while holding the total number of individuals constant results in small within-deme populations for which even the minimum sample size of 1 approaches the local N_e (Table A1). This results in an excess of short terminal branches in the coalescent tree, which decreases the total branch length and leads to fewer segregating sites, deflated θ_W, and inflated Tajima's D. Overall, the stepping-stone model reproduces important features of spatial structure in our continuous space model, such as a decline in θ_π and correlations between spatial and genetic distance with increasing migration, but introduces artifacts caused by binning the landscape into discrete demes.

Demographic Model

Local population regulation is controlled by two parameters, L and K. Here, we show that these should be close to the average life span of an individual and the average number of individuals per unit area, respectively. We chose our demographic model so that every individual has on average $1/L$ offspring each time step, and if the local population density of an individual is n, then their probability of survival until the next time step is:

$$p = \min\left(0.95, \frac{1}{1 + n/\big(K(1+L)\big)}\right). \tag{A1}$$

Table A1 Stepping-stone simulation parameters

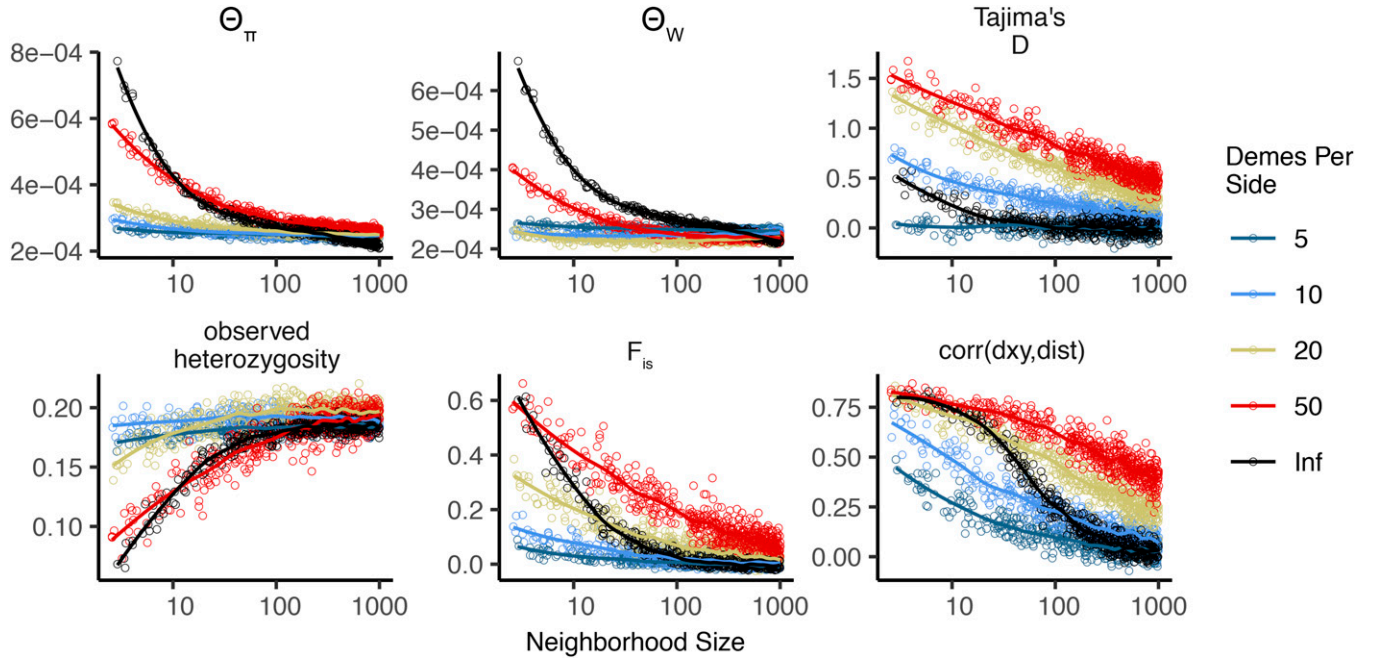| Demes per side (n)	N_e per deme	Samples per deme
5	244	20
10	61	10
20	15.25	2
50	2.44	1

Figure A1 Summary statistics for two-dimensional coalescent stepping-stone models with fixed total N_e and varying numbers of demes per side. The black "infinite" points are from our forward-time continuous space model. Interdeme migration rates are related to σ as described above.

We capped survival at 0.95 so that we would not have exceptionally long-lived individuals in sparsely populated areas, otherwise an isolated individual might live for a very long time. Since $1 - p \approx n/(K(1 + L))$, mortality goes up roughly linearly with the number of neighbors (on a scale given by K), as would be obtained if, for instance, mortality is due to agonistic interactions. Ignoring migration, a region is at demographic equilibrium if the per-capita probability of death is equal to the birth rate, *i.e.*, if $1 - p = 1/L$ (note that there is no effect of age in the model, which would make the analysis more complicated). Solving this for n, we get that in a well-mixed population, the equilibrium density should be around

$$n = K\frac{L+1}{L-1} \tag{A2}$$

individuals per unit area. At this density, the per-capita death rate is $1/L$, so the mean lifetime is L. This equilibrium density is *not* K, but (since $L = 4$) is two-thirds larger. However, in practice this model leads to a total population size that is around K multiplied by total geographic area (but which depends on σ, as discussed above). The main reason for this is that since offspring tend to be near their parents, individuals tend to be "clumped," and so experience a higher average density than the density one would compute by dividing census size by geographic area (Lloyd 1967). To maintain a constant expected total population size would require making (say) K depend on σ; however, typical local population densities might then be more dissimilar.

Do you want to participate in the Author's Choice Open Access option for your article?

☐ No
☐ Yes, Standard Open Access
☐ Yes, Creative Commons CC BY 4.0 License

Both Author Choice Open options make your article freely available to all readers (regardless of subscription) immediately after publication. With the Standard Author Choice Open Access, copyright remains with the Genetics Society of America as outlined in our copyright policy and future re-use of your content by others requires permission from GSA. With the CC BY 4.0 option, you hold copyright on the article, but anyone can share or adapt for any purpose, even commercially so long as they attribute the original source. Some authors have explained that they do not wish to grant others the right to modify and/or sell their content, so we offer both choices for the content to be made freely-available. Both Open Access options carry a surcharge of $1500 for GSA members or $2000 for non-members

More information: http://www.genetics.org/content/after-acceptance#charges

QA1 If you or your coauthors would like to include an ORCID ID in this article, please provide your respective ORCID IDs along with your corrections.

Note: If you do not yet have an ORCID ID and would like one, you may register for this unique digital identifier at https://orcid.org/register.

1 Please verify corresponding author address.

2 Please confirm or update any and all URLs in your article.

3 Please verify all Supplemental Material links in your article.

4 Please verify styling of Greek and math symbols in text and equations throughout article. Check carefully for correct use of boldface, italics, operators, qualifiers, spacing, superscripts, and subscripts. Journal style includes Greek letters set roman (not italic), math variables set in italics, and variable modifiers set in roman.

5 Any alternations between capitalization and/or italics in genetic and taxonomic nomenclature have been retained per the original manuscript. *Genetics* style is for genes and alleles to be italicized; please confirm that all nomenclature has been formatted properly throughout. Per journal style, uppercase Greek letters should remain roman even when appearing in a term where the overall style is italic (e.g., a gene name such as *kap108Δ*). Note that headings are set all roman or all italics based on journal style and should not be changed.

6 Please check all figure legends carefully to confirm that any and all labels, designators, directionals, colors, etc. are represented accurately in comparison with the figure images.

7 Per journal style, the word "preprint" must appear after the year in any in-text preprint citations. Please amend any in-text citations as necessary.

8 Please provide zipcode for affiliation and corresponding author.

9 If an abbreviation, please define "SLiM" at first mention.

10 A required subsection at the end of the Materials and Methods entitled "Data availability" has been added per journal style. Please confirm that this statement is accurate, or if not, update to include the details of where your data can be found. Details are available in the Materials and Methods instructions at http://www.genetics.org/content/prep-manuscript#text.

11 Please provide complete details for reference "Miles and Harding (2017)."

12 Please provide complete details for reference "Ralph *et al.* (2019a)."

13 Please provide complete details for Ref. "Wilke (2019)."

14 If abbreviations, please define "nIBS" and "dxy" in the legend for Figure 4.